TECHNICAL REPORT BRL-TR-3223

BRL

JET BREAKUP AND COMBUSTION MODELING FOR THE REGENERATIVE LIQUID PROPELLANT GUN

TERENCE P. COFFEE
PAUL G. BAER
WALTER F. MORRISON
GLORIA P. WREN

APRIL 1991

U.S. ARMY LABORATORY COMMAND

BALLISTIC RESEARCH LABORATORY
ABERDEEN PROVING GROUND, MARYLAND

NOTICES

Destroy this report when it is no longer needed. DO NOT return it to the originator.

Additional copies of this report may be obtained from the National Technical Information Service, U.S. Department of Commerce, 5285 Port Royal Road, Springfield, VA 22161.

The findings of this report are not to be construed as an official Department of the Army position, unless so designated by other authorized documents.

The use of trade names or manufacturers' names in this report does not constitute indorsement of any commercial product.

REPORT DOCUMENTATION PAGE

Form Approved
OMB No 0704-0188

1. AGENCY USE ONLY (Leave blank)	2. REPORT DATE	3. REPORT TYPE AND DATES COVERED
	April 1991	Final, Feb 89 - Dec 89

4. TITLE AND SUBTITLE
Jet Breakup and Combustion Modeling for the Regenerative Liquid Propellant Gun

5. FUNDING NUMBERS
DA306132
IFVM9Y9XA450

6. AUTHOR(S)
Terence P. Coffee, Paul G. Baer, Walter F. Morrison, and Gloria P. Wren

7. PERFORMING ORGANIZATION NAME(S) AND ADDRESS(ES)
U.S. Army Ballistic Research Laboratory
ATTN: SLCBR-IB-B
Aberdeen Proving Ground, MD 21005-5066

8. PERFORMING ORGANIZATION REPORT NUMBER

9. SPONSORING/MONITORING AGENCY NAME(S) AND ADDRESS(ES)
U.S. Army Ballistic Research Laboratory
ATTN: SLCBR-DD-T
Aberdeen Proving Ground, MD 21005-5066

10. SPONSORING/MONITORING AGENCY REPORT NUMBER
BRL-TR-3223

11. SUPPLEMENTARY NOTES

12a. DISTRIBUTION/AVAILABILITY STATEMENT
Approved for public release; distribution is unlimited.

12b. DISTRIBUTION CODE

13. ABSTRACT (Maximum 200 words)

Although interior ballistic models of the regenerative liquid propellant gun have been shown to be capable of accurately describing the mechanical response of the system, descriptions of the breakup and combustion of the liquid jet have proven less satisfactory. The propellant has been assumed to break into droplets whose diameters are functions of piston position or chamber pressure, and then combust according to a pressure-dependent burn rate law. This empirical description of the jet breakup has been shown to provide accurate gun simulations and to be reasonably predictive in terms of maximum pressure and muzzle velocity within guns of the same caliber. However, it has previously not been possible to identify a unifying set of parameters which describes breakup and combustion among calibers.

Therefore, this report explores the adaptability of models of jet breakup discussed in the literature to the regenerative liquid propellant gun environment. A particular model is chosen and implemented in the lumped parameter gun code. With a single value of the one adjustable parameter, the model accurately simulates experimental data from all three Concept VIC gun calibers. An alternate approach is also derived that does not involve droplets. The agreement between the two new models is excellent.

14. SUBJECT TERMS	15. NUMBER OF PAGES
liquid gun propellants, regenerative gun, atomization, Concept VIC, lumped parameter model, monopropellants	47
	16. PRICE CODE

17. SECURITY CLASSIFICATION OF REPORT	18. SECURITY CLASSIFICATION OF THIS PAGE	19. SECURITY CLASSIFICATION OF ABSTRACT	20. LIMITATION OF ABSTRACT
UNCLASSIFIED	UNCLASSIFIED	UNCLASSIFIED	UL

INTENTIONALLY LEFT BLANK.

TABLE OF CONTENTS

		Page
	LIST OF FIGURES	v
	LIST OF TABLES	vii
1.	INTRODUCTION	1
2.	PRESENT METHODS	2
3.	MODELING ASSUMPTIONS	4
4.	INJECTION MODELS	5
5.	NUMERICAL IMPLEMENTATION	7
6.	RESULTS - INJECTION MODEL	9
7.	OTHER SIMULATIONS	11
8.	INTACT JET CORE	13
9.	SENSITIVE TIME LAG MODEL	16
10.	RESULTS - TIME LAG MODEL	18
11.	SUMMARY	19
12.	REFERENCES	35
	GLOSSARY	38
	DISTRIBUTION LIST	41

INTENTIONALLY LEFT BLANK.

LIST OF FIGURES

Figure		Page
1.	A Concept VIC Regenerative Liquid Propellant Gun	20
2.	Combustion Chamber Pressure, 30-mm Gun, Experiment (line), Instantaneous Combustion Model (dot), 30-mm Droplet Profile (dash)	21
3.	Combustion Chamber Pressure, 105-mm Gun, Experiment (line), Instantaneous Combustion Model (dot), 30-mm Droplet Profile (dash)	21
4.	Combustion Chamber Pressure, 155-mm Gun - 2-Liter Charge. Experiment (line), Instantaneous Combustion Model (dot), 30-mm Droplet Profile (dash)	22
5.	Combustion Chamber Pressure, 155-mm Gun - 5-Liter Charge. Experiment (line), Instantaneous Combustion Model (dot), 30-mm Droplet Profile (dash)	22
6.	Empirical Droplet Diameter Profiles, 30-mm (line). 105-mm (dot). 155-mm - 2-Liter Charge (dash), 155-mm - 5-Liter Charge (dot-dash)	23
7.	Combustion Chamber Pressure, 30-mm Gun. Experiment (line). Droplet Injection Model (dot)	23
8.	Combustion Chamber Pressure, 105-mm Gun. Experiment (line). Droplet Injection Model (dot)	24
9.	Combustion Chamber Pressure, 155-mm Gun - 2-Liter Charge. Experiment (line), Droplet Injection Model (dot)	24
10.	Combustion Chamber Pressure, 155-mm Gun - 5-Liter Charge. Experiment (line), Droplet Injection Model (dot)	25
11.	Droplet Injection Model, 155-mm Gun - 5-Liter Charge. Injected Droplet Diameter (line), Combustion Chamber Droplet Diameter (dot)	25
12.	Droplet Injection Model, Combustion Chamber Droplet Diameter Profiles. 30-mm (line), 105-mm (dot), 155-mm - 2-Liter Charge (dash), 155-mm - 5-Liter Charge (dot-dash)	26
13.	Combustion Chamber Pressure, 30-mm Gun - Round 15. Experiment (line), Droplet Injection Model (dot)	26
14.	Combustion Chamber Pressure, 30-mm Gun - Round 22. Experiment (line), Droplet Injection Model (dot)	27

Figure		Page
15.	Combustion Chamber Pressure, 105-mm Gun - Round 15. Experiment (line), Droplet Injection Model (dot)	27
16.	Combustion Chamber Pressure, 105-mm Gun - Round 7. Experiment (line), Droplet Injection Model (dot)	28
17.	Combustion Chamber Pressure, 155-mm Gun - Round 17. Experiment (line), Droplet Injection Model (dot)	28
18.	Combustion Chamber Pressure, 155-mm Gun - Round 58. Experiment (line), Droplet Injection Model (dot)	29
19.	Combustion Chamber Pressure, 155-mm Gun - Round 65. Experiment (line), Droplet Injection Model (dot)	29
20.	Combustion Chamber Pressure, 30-mm Gun - Concept VI - Round 8. Experiment (line), Droplet Injection Model (dot)	30
21.	Liquid Accumulation, 30-mm Gun. Simulation (line), Taylor (dot), Wolfe and Andersen times 10 (dash), Mayer times 100 (dot-dash)	30
22.	Liquid Accumulation, 155-mm Gun - 5 Liter Charge. Simulation (line), Taylor divided by 5 (dot), Wolfe and Andersen times 3 (dash), Mayer Times 25 (dot-dash)	31
23.	Combustion Chamber Pressure, 30-mm Gun. Experiment (line), Droplet Injection Model (dot), Sensitive Time Lag Model (dash)	31
24.	Combustion Chamber Pressure, 105-mm Gun. Experiment (line), Droplet Injection Model (dot), Sensitive Time Lag Model (dash)	32
25.	Combustion Chamber Pressure, 155-mm Gun - 2-Liter Charge. Experiment (line), Droplet Injection Model (dot), Sensitive Time Lag Model (dash)	32
26.	Combustion Chamber Pressure, 155-mm Gun - 5-Liter Charge. Experiment (line), Droplet Injection Model (dot), Sensitive Time Lag Model (dash)	33

LIST OF TABLES

Table		Page
1.	Muzzle Velocities Assuming Instantaneous Combustion	2
2.	Muzzle Velocities Using the 30-mm Droplet Profile	3
3.	Muzzle Velocities Using the New Droplet Profile	10
4.	Muzzle Velocities Using the New Droplet Profile - Other Simulations	12
5.	Muzzle Velocities Using the Sensitive Time Lag Model	18

INTENTIONALLY LEFT BLANK.

1. INTRODUCTION

Regenerative liquid propellant gun (RLPG) technology is sufficiently mature to allow the testing of the first 155-mm liquid propellant gun fixture. In support of the development of this artillery weapon, test fixtures in 30 mm and 105 mm sizes have been built and fired. The data from all these fixtures have been extensively analyzed to better understand the RLPG process (Coffee, Wren, and Morrison 1989, 1990; Wren, Coffee, and Morrison 1990). Previous reports describe the design of the Concept VIC gun fixtures and the modeling modifications pertinent to this design. Agreement between the interior ballistics simulations and the experimental data is quite good. Details of the lumped parameter gun code used for these simulations have been described in previous publications (Coffee 1985; Coffee 1988; Morrison and Coffee 1990).

A Concept VIC RLPG is shown in Figure 1. An external solid or liquid propellant igniter venting into the combustion chamber initiates the ballistic cycle. The chamber pressure forces both the control and injection pistons rearward. Liquid propellant is then injected from the liquid reservoir through the annulus between the pistons into the combustion chamber where it burns. Typically, the startup regime of the RLPG process is characterized by accumulation of liquid propellant in the combustion chamber in an unreacted or partially reacted state. Combustion models have been implemented to simulate this delay in energy release.

The most unsatisfactory aspect of the interior ballistics simulations is the combustion model. The mean diameter of the droplets in the combustion chamber is input as a function of pressure. The droplets then combust according to a pressure dependent burning rate law, which is based on experimental burning rate data (McBratney 1980, 1981). The optimum droplet profile must be derived for each case. The droplet profiles for different initial conditions, and especially for different calibers, vary substantially in magnitude, although their qualitative behavior is similar.

In this paper, we discuss procedures for predicting the droplet profiles. Input parameters are kept the same as in the most accurate model from the previous reports. Only the combustion model is varied.

A total of eleven different experimental cases were considered in the three simulation reports (Coffee, Wren, and Morrison 1989, 1990; Wren, Coffee, and Morrison 1990). This report will concentrate on the four repeatability series. These were sets of test firings in which the initial conditions were as identical as possible. The experimental muzzle velocities show excellent repeatability (standard deviations less than half a percent), although the pressures show more variation. The average muzzle velocities for the repeatability series are presented in Table 1.

2. PRESENT METHODS

One option built into the interior ballistics code is an assumption of instantaneous propellant combustion. The assumption is made that the liquid propellant releases all its energy immediately upon injection into the combustion chamber. This is the limiting case of very rapid combustion. Table 1 shows the muzzle velocities predicted using this assumption. Results are given for the four repeatability series. Agreement is quite good, although not quite as accurate as the desired modeling goal of two percent (Coffee, Wren, and Morrison 1989).

Table 1. Muzzle Velocities Assuming Instantaneous Combustion

Gun	Charge, l	Muzzle Velocity, Exp (m/s)	Muzzle Velocity, Model (m/s)	Percent difference
30-mm	.23	776	757	-2.5
105-mm	2.0	666	654	-1.8
155-mm	2.2	393	407	3.6
155-mm	5.2	586	595	1.5

Figures 2-5 show the experimental chamber pressures (solid line) for the four repeatability series, compared to a simulation using instantaneous combustion (dotted line). It is noted that there is substantial disagreement in the experimental pressures recorded at the different gauge locations. This is assumed to be due to calibration errors and thermal drift. Thus the experimental pressure curves shown are those that appear to be most consistent with the overall experimental results (Coffee, Wren, and Morrison 1989, 1990; Wren, Coffee, and Morrison 1990). Although the maximum pressure is predicted to 8% in the worst case

(30 mm), the simulations using the instantaneous combustion model show poor agreement with the shape of the experimental pressure profiles. The simulations show the primary pressure rise occurring early due to the unrealistically high propellant gas generation rate at low pressure, indicating that liquid accumulation is important in these shots.

One method of including the effect of accumulation is to derive a droplet diameter profile as a function of pressure for each case (Coffee, Wren, and Morrison 1989, 1990; Wren, Coffee, and Morrison 1990). In general, the use of a droplet diameter profile results in accurate simulation of the experimental chamber pressure profile. However, the resulting droplet diameter profiles for the four cases in Table 1 vary considerably, as shown in Figure 6. Although the droplet diameters decrease with pressure in all cases, the authors were unable to develop a unifying set of parameters for the four cases which generates the desired droplet diameters.

As an alternative to the instantaneous combustion model and the individual droplet diameter profile approaches, a droplet profile derived for one case may be applied to the simulation of other cases. The use of a droplet profile from another case does improve the overall interior ballistic simulation in comparison to the instantaneous combustion model. As an illustration, the droplet profile derived for the 30-mm case is applied to the other three cases. The simulated muzzle velocities are presented in Table 2. Agreement is, of course, excellent for the 30-mm case, but agreement is also improved for the other three cases. Muzzle velocity predictions are within the 2% range.

Table 2. Muzzle Velocities Using the 30-mm Droplet Profile

Gun	Charge, l	Muzzle Velocity, Exp (m/s)	Muzzle Velocity, Model (m/s)	Percent difference
30-mm	.23	776	776	0.0
105-mm	2.0	666	663	-0.5
155-mm	2.2	393	389	-1.0
155-mm	5.2	586	596	1.7

Figures 2–5 show the comparison of pressure vs. time curves for these simulations (dashed lines) with experimental data. Agreement in Figure 2 is quite good, as expected. Disagreement after peak pressure is in part due to thermal drift in the pressure gauge. In the 105-mm case (Figure 3), the position of the rapid pressure rise is approximately correct, but the slope of the curve is too large in the simulation. Nevertheless, this is a credible simulation. In the 155-mm, 2-liter case (Figure 4), the simulation is quite poor. Since this shot is a very low pressure test, only the initial portion of the 30-mm droplet diameter profile is used. For the higher pressure 155-mm case (Figure 5), overall agreement is improved, although the initial part of the pressure rise (5 to 10 ms) is not simulated well. The maximum difference in the peak pressures between experiment and simulation is about 6% (105-mm case).

3. MODELING ASSUMPTIONS

Our goal is to obtain a more fundamental model of the injection and combustion processes. The liquid propellant is injected as an annular jet at high velocity into a hot, high density gas. Both the velocity and the thickness of the jet change rapidly with time. The jet is assumed to break up into droplets. These drops can break up further or they can coalesce. The droplets are heated and eventually ignite. The droplets then combust and release the propellant energy. A number of assumptions are required to make the problem tractable.

We assume that the liquid propellant instantaneously forms droplets as it enters the combustion chamber. Under gun conditions (very high velocities), the jet is expected to be in the atomization regime, i.e., droplets begin forming immediately upon entry into the chamber. While some liquid will remain in the jet core, the amount is assumed to be small (see below).

The droplets are assumed to begin to combust instantaneously, i.e., droplet heating and ignition is ignored. The droplets are assumed to burn according to an experimental, pressure dependent, linear regression rate (McBratney 1980, 1981). The gas generation rate then depends only on the pressure and the total surface area of the droplets. The ignition systems in the VIC configurations produce a highly turbulent, hot, high pressure environment in the gun chamber; therefore, this should be a good approximation.

The liquid propellant burning rate has only been measured up to about 100 MPa (McBratney 1981). The data indicates a break in the slope of the burning rate above 60 MPa, but the rates measured at the higher pressures are considered less reliable. Therefore, only the rates measured up to 60 MPa are used to derive the fit to the burning rate data, and this fit is extrapolated to higher pressures.

Essentially all studies of jet breakup have been carried out under steady state conditions. We assume that steady state models still apply under gun conditions. Injection velocities and chamber conditions change rapidly during a gun firing. However, if the jet breakup is rapid enough, this will not be an important effect.

When a jet breaks up, a distribution of droplet sizes will be created. We assume that all the droplets created are of the same size, representing a mean diameter. This diameter is chosen to be the Sauter mean diameter, which preserves both volume and surface area of a droplet distribution.

Jet breakup depends heavily on the relative velocity between the liquid and the gas. However, in the simulation, the chamber gas is assumed to be stagnant since the actual gas flow pattern in the chamber is unknown.

Once the droplets are formed, they are assumed not to interact with one another. This is probably the weakest assumption. The liquid propellant spray in the gun is very dense. Droplet combustion is known to depend upon neighborhood conditions (Faeth 1983). Also, droplets could coalesce into larger droplets. Since the injection velocity is increasing over the first part of the firing cycle, later injected liquid could easily catch up to liquid injected earlier in the ballistic cycle and form a dense liquid "clump." This effect is ignored only because we have no way of taking it into account.

4. INJECTION MODELS

Weiss and Worsham (1959) performed a series of experiments in which molten wax was injected through circular holes into steady high velocity airstreams. The experimental droplet diameter could be correlated quite well by the relation

$$d = .5978\ V^{-4/3}\ v^{1/12}\ D^{1/6}\ \sigma_L^{5/12}\ \mu_L^{1/3}\ \mu_G^{1/12}\ \rho_L^{1/6}\ (1/\rho_G + 1/\rho_{GO}), \quad (1)$$

where V is the relative velocity between the gas and liquid (cm/s), v is the absolute velocity of the liquid (cm/s), D is the injection hole diameter (cm), σ_L is the surface tension of the liquid (dynes/cm), μ_L is the liquid dynamic viscosity (poise), μ_G is the gas dynamic viscosity (poise), ρ_L is the liquid density (g/cc), ρ_G is the gas density (g/cc), and ρ_{GO} is the gas density at atmospheric pressure and room temperature (g/cc). Equation 1 is in a different form than reported by Weiss and Worsham to better show the functional relationships. In the original paper the parameters were organized into non-dimensional groups. The diameter reported is the mass mean diameter of the measured droplets. In these experiments the liquid velocity was much smaller than the gas velocity, so the contribution of the absolute liquid velocity term is negligible. Weiss and Worsham concluded that the atomization occurs by direct action of the airstream on the exposed liquid surface. Therefore, the relative velocity, V, between liquid and gas is of primary importance.

A later paper by Mayer (1961) presented a theoretical approach to the atomization problem. Mayer assumed that capillary waves (ripples) are produced by a high velocity gas flow along the liquid surface. Waves of very small wavelength cannot be developed readily because of viscous dissipation. Waves of very long wavelength are slow to develop because of inertial effects. There then exists a spectrum of intermediate wavelengths which can be excited to appreciable amplitudes. Eventually, the gas stream will produce a ligament of liquid by stripping of the wavecrest, from which droplets of diameter comparable in size to the wavelength are formed. Mayer obtained a formula for the resulting mean droplet size

$$d = 21.37\ V^{-4/3}\ \sigma_L^{1/3}\ \mu_L^{2/3}\ \rho_L^{-1/3}\ \rho_G^{-2/3}. \quad (2)$$

This formula does not include the small dependence on injection diameter or the very small dependence on absolute liquid velocity and gas viscosity. Moreover, the form of the density dependence is completely different. However, Mayer noted that the Weiss and Worsham data could be correlated by using the gas density to the -2/3 power, rather than the form actually chosen by Weiss and Worsham (1959). The Weiss and Worsham liquid density relation was obtained by dimensional analysis, not from experiment. That is, the 1/6 power on the liquid density was chosen so the formula for the diameter has the proper units. If the gas density

exponent in the Weiss and Worsham formula is changed to -2/3, then the liquid density must have an exponent of -1/6. So the Weiss and Worsham formula is similar to the Meyer formula.

A later report by Wolfe and Andersen (1964) presented an alternative derivation of liquid breakup. While presented in terms of droplet breakup, the same general ideas apply to jet breakup. As in the description above, aerodynamic forces strip off blocks of liquid. But Wolfe and Andersen also take into account the curvature of the droplet. They obtain

$$d = 5.1426\ V^{-4/3}\ D^{1/6}\ \sigma_L^{1/2}\ \mu_L^{1/3}\ \rho_L^{-1/6}\ \rho_G^{-2/3}, \tag{3}$$

where D is the diameter of the original large drop. Since this is a curvature effect, the outer diameter of the annular jet should be used, rather than the hydraulic diameter of the jet.

All three formulas are similar. We would like to know if they are likely to be valid under gun conditions. The experimental velocities, viscosities, and surface tension studied are similar to those expected in the gun. The diameter of the gun annular jet is substantially larger than the circular jets (and droplets) used for the above correlations. The initial gas density in the gun is small, but increases to a couple of orders of magnitude larger than the cases studied by the above authors. Due to the difference in conditions, it was felt better to extrapolate a theoretical formulation rather than the purely experimental correlation of Weiss and Worsham. The Wolfe and Andersen formula was chosen since it takes into account the diameter of the jet, which varies substantially as the gun caliber is changed.

5. NUMERICAL IMPLEMENTATION

Equation 3 gives the diameter of the drops injected into the combustion chamber at a given time, whereas the gun code requires the Sauter mean diameter of all the drops in the chamber. To implement the new correlation, an ordinary differential equation for the surface area, S_3, of all the liquid in the combustion chamber is introduced. There are two drop diameters: the injected drop diameter, d_j, and the Sauter mean diameter, d_3, of the drops already in the chamber. At any given time step, the rate of change of the surface area depends on the rate at which surface area is being introduced from the injected droplets

minus the rate at which surface area is decreasing due to combustion. After each time step, the new Sauter mean diameter in the chamber is obtained from the known surface area, liquid density, and liquid mass. The relation between the surface area and the mean diameter is given by

$$S_3 = \frac{6M_{L3}}{\rho_{L3}d_3} , \tag{4}$$

where M_{L3} is the mass of all the liquid in the chamber, and ρ_{L3} is the density of the liquid in the chamber. The governing equation for the chamber surface area is

$$\frac{dS_3}{dt} = \frac{6m_{13}}{\rho_{L3}d_j} - \frac{4m_3}{\rho_{L3}d_3} - \frac{6m_{34}}{\rho_{L3}d_3}\frac{M_{L3}}{M_3} , \tag{5}$$

where m_{13} is the rate of mass injection from the reservoir (g/s), m_3 is the rate of combustion of the liquid in the chamber (g/s), m_{34} is the rate of injection of mass into the gun tube (g/s), and M_3 is the total mass (liquid and gas) in the chamber. The first term in Equation 5 follows directly from Equation 4. The rate of change of surface area depends on how rapidly droplets of a specified size are being injected. The last term is exactly analogous, and accounts for the loss of droplets to the gun tube. Only that fraction of the total mass injected into the tube that is liquid is relevant. The middle term accounts for the decrease in surface area due to combustion. The combustion process causes the droplet diameter to decrease linearly depending on the pressure dependent burn rate. Surface area will also change due to changes in liquid density, but this effect is very small and is ignored.

The surface area Equation 5 is not strictly correct. The derivation assumes that the drops in the chamber are all actually of the same size, rather than just having a specified Sauter mean diameter. However, the surface area is only required to compute the rate at which the liquid is combusting. Given the uncertainties in the burning rate and the injected droplet size, the relation is believed to be sufficiently accurate.

There are analogous equations for the gun tube. When droplets are injected into the gun tube, the change in pressure causes a slight change in density, and hence in droplet size. So the size of the droplets, d_{j4}, injected into the gun tube is given by

$$d_{j4} = d_3 \, (\rho_{L3} / \rho_{L4})^{1/3}, \tag{6}$$

where ρ_{L4} is the average density of the liquid in the gun tube (g/cc). The equation for the surface area, S_4, in the tube is

$$\frac{dS_4}{dt} = - \frac{4m_4}{\rho_{L4} d_4} + \frac{6m_{34}}{\rho_{L4} d_{j4}} \frac{M_{L3}}{M_3}, \tag{7}$$

where m_4 is the rate of combustion of the liquid in the tube (g/s), and d_4 is the average droplet diameter of the drops in the tube (cm).

The other equations in the code are unchanged (Coffee 1985, 1988).

6. RESULTS - INJECTION MODEL

The Wolfe and Andersen formula was implemented in the gun code. The code predicts small droplets, and the resulting pressure-time curve is very close to that resulting from the instantaneous combustion model. Although the simulation is disappointing, the standard steady state breakup models may not apply under the highly transient, very dense conditions of the gun. Alternately, the problem may be a delay in the formation of droplets from the jet. This latter process will be examined in a following section on intact jet core models.

However, it is still possible that the functional relationship is a reasonable approximation to gun conditions. Thus, a scaling factor is introduced and benchmarked against the 30 mm case. If the droplet diameter is multiplied by 30, a reasonable approximation to the chamber pressure is obtained (Figure 7). The agreement is not impressive, but the simulation does reflect the correct shape and magnitude of the experimental curve.

The model is then applied to the other three cases with the same scaling factor. The agreement in all three cases is very good with no additional fine tuning of the injection model (Figures 8–10). The agreement in muzzle velocity is also quite good (Table 3). The largest disagreement in the maximum chamber pressure is only 2.4% (30-mm case).

Table 3. Muzzle Velocities Using the New Droplet Profile

Gun	Charge, l	Muzzle Velocity, Exp (m/s)	Muzzle Velocity, Model (m/s)	Percent difference
30-mm	.23	776	767	-1.2
105-mm	2.0	666	658	-1.2
155-mm	2.2	393	399	1.5
155-mm	5.2	586	593	1.2

The results are encouraging. All four cases are well represented by the same droplet model with the same value for the single adjustable parameter.

In general, the injected droplet diameter is nearly the same as the average droplet diameter in the chamber (Figure 11). During the early injection process, the injected droplet diameter decreases more rapidly than the diameter of the droplets in the chamber, which is decreasing due to combustion. As the injected droplet diameter levels off, this relationship is reversed.

In Figure 12, the new chamber droplet diameter profiles for the four cases in Table 3 vs. the chamber pressure are compared. At early times the droplets are large (upper left corner of graph). As the pressure increases the droplets decrease in size (lower right corner). Finally, as the pressure drops off, the droplets increase slightly in size (lower left corner). Although there are differences among the curves in Figure 12, the profiles of injected droplet diameters show more similarity than the previously derived profiles (Figure 6) of the mean diameter of droplets in the chamber. The similarity among the curves in Figure 12 is related to the fact that all the guns considered here have almost the same hydraulic difference between the liquid reservoir and the combustion chamber. Hence, the guns have similar injection velocities as a function of chamber pressure. The liquid and gas density, viscosity,

and surface tension are nearly the same in all four cases. Thus, since the injected droplet diameter predicted by Equation 3 depends most heavily on the injection velocity, the droplet profiles in Figure 12 are very similar.

The case which appears most different in Figure 12 is the 155-mm gun, 2-liter charge, in which the peak pressure occurs at about 60 MPa. However, the behavior of the injected droplet diameter curve is still similar to the other three cases. Maximum pressure is simply much lower than for the 30-mm, 105-mm, or 155-mm, 5-liter firings. In addition, for this case injection continues as the pressure falls to lower values. The fact that the profiles in Figure 6 and the profiles in Figure 12 both result in accurate simulations indicates that the combustion chamber pressure is not highly sensitive to small changes in the droplet profile.

7. OTHER SIMULATIONS

The new model works quite well for the four repeatability series. For completeness, the model is also applied to the other VIC firings that have been studied.

Two early firings of the 30-mm VIC fixture have been analyzed (Coffee, Wren, and Morrison 1989). A comparison of experimental and predicted chamber pressure for Round 15 is shown in Figure 13. The droplet injection model does result in accurate prediction of the muzzle velocity (Table 4). However, it does not provide as good a simulation of the experimental chamber pressure. In the simulation, the chamber pressure increase occurs too late. If the simulation curve is shifted slightly in time, the agreement between simulation and experiment is quite good. A common zero time between the experimental and predicted pressure curves can usually be obtained by comparing the piston travel curves. However, for these early 30-mm shots, the piston travels were not recorded successfully, and a common zero time cannot be established. Thus, the accuracy of the injection model cannot reliably be assessed. The same general behavior is exhibited in the simulation of the other 30-mm shot (Figure 14).

Figure 15 shows the experimental and simulated chamber pressures for an early 105-mm shot. In this case, the simulated pressure rises substantially earlier than the actual pressure. Since the piston travel measurements are accurate for this case, this is a genuine effect.

Table 4. Muzzle Velocities Using the New Droplet Profile - Other Simulations

Gun	Round	Muzzle Velocity, Exp (m/s)	Muzzle Velocity, Model (m/s)	Percent difference
30-mm	15, 22	622, 547	613, 537	-1.4, -1.8
105-mm	15, 7	540, 391	542, 394	.4, .8
155-mm	17, 58, 65	424, 596, 683	425, 595, 683	.2, -.2, .0

Figure 16 shows the chamber pressures for another 105-mm shot. In this case, the pressure rise occurs at the proper time, but the predicted maximum chamber pressure is high. The model does not match the pressure curves very well for these cases. However, the predicted muzzle velocities are extremely accurate (Table 4).

Figure 17 shows the results for an early 2-liter shot for the 155-mm gun. The agreement is not quite as good as for the repeatability series. Figure 18 shows the results for a 5-liter shot fired after the repeatability series using the new hybrid igniter. Agreement is reasonable. Figure 19 shows the results for an early 7-liter firing. The simulated and experimental pressure curves agree quite well. Muzzle velocities are predicted very accurately for all three cases (Table 4). The muzzle velocities for the last two cases are given at 200 inches of projectile travel rather than at muzzle exit.

An earlier experimental 30-mm gun fixture at the BRL, referred to as a Concept VI configuration, has been examined in some detail (Coffee 1988). This concept features a stationary center bolt, one moving outer piston, and no damper. Figure 20 shows the results of applying the new droplet injection model. The initial agreement in pressure is quite good. However, the simulation shows a rapid pressure rise while the experimental chamber pressure levels off. The predicted muzzle velocity (1,183 m/s) is in very poor agreement with the experimental muzzle velocity (1,020 m/s).

The above simulations have shown that our droplet model is not a universal solution. Evidently, for the 30-mm Concept VI gun fixture, the liquid does not combust as rapidly as the model predicts. Some of the mechanisms ignored in the development of the droplet model are undoubtably important. However, the model does give good agreement with all the Concept VIC experimental results, and appears to provide some predictive capability for this gun design.

8. INTACT JET CORE

The various droplet models studied predict very small droplets under gun conditions, and the droplet diameters must be multiplied by a constant to obtain agreement with experiment. This raises the question of whether immediate droplet formation is the most appropriate physical model in the gun environment. It is expected that some liquid will be in the intact core of the injected liquid jet. In this section, we assess whether the experimental results can be better explained by assuming that most of the liquid accumulation is in the form of an intact core of the jet.

Mayer (1961) also developed a formula for the breakup time of the jet. His result can be written in the form

$$t_b = 0.2356\ D_h\ V^{-4/3}\ \sigma_L^{1/3}\ \mu_L^{-1/3}\ \rho_L^{2/3}\ \rho_G^{-2/3}, \tag{8}$$

where D_h is the hydraulic diameter of the annular injector. The length of the intact core can be approximated by multiplying the breakup time t_b times the injection velocity V (ignoring drag). Assuming the intact core is cone shaped, the volume is approximately

$$Vol = 0.5\ V\ t_b\ A_v, \tag{9}$$

where A_v is the vent area of the injector.

Wolfe and Andersen (1964) developed a similar formula,

$$t_b = D_h / [\ (A^2 + B\ P)^{1/2} - A], \tag{10}$$

where

$A = 16\ \mu_L / D_h\ \rho_L$

$B = 2 / \rho_L$

$P = 0.5\ \rho_G\ V^2 - 2\ \sigma_L / D_h.$

The authors note that if the viscous and surface tension forces are negligible, this reduces to

$$t_b = D_h V^{-1} \rho_L^{1/2} \rho_G^{-1/2}. \quad (11)$$

Chatwani and Bracco (1985) report a breakup length formula based on the theory of Taylor. The breakup length is

$$x_b = (1.75 / f_m) D_h \rho_L^{1/2} \rho_G^{-1/2}, \quad (12)$$

where f_m is a numerically computed quantity less than one and the constant 1.75 was chosen based on comparison with experiment. This is, in fact, identical with the simplified Wolfe and Andersen formula, except for the $1.75/f_m$ term.

All three of the formulas were implemented in a small post-processor code. That is, first the standard gun code is run. The parameter values required by the intact core models, such as injection velocity, vent area, etc., are read in from the output of the gun code simulation. These are considered to be reasonably accurate because of the agreement of the gun code results with experiment. Then the post-processor code, using the values from the gun code in the above formulas, computes the mass in the intact core. Figure 21 shows the results for a 30-mm firing. The solid line is the liquid accumulation from a simulation of the 30-mm Concept VIC gun (dotted line in Figure 6). The dotted line is the accumulation resulting from the application of the Taylor formula (Equation 12). The dashed line gives the Wolfe and Andersen result, Equation 10, multiplied by 10, and the dotted-dashed line the Mayer result, Equation 8, multiplied by a 100. The results were multiplied by a constant to obtain the proper order of magnitude for the accumulation.

The computation of the intact jet length is only approximate. A comparison of the predicted accumulation in Figure 21 emphasizes the scatter in the three formulas. According to the Mayer formula, Equation 8, the liquid core is negligible. According to the Wolfe and Andersen formula, Equation 10, the liquid core is at times a noticeable amount of the liquid accumulation. According to the Taylor formula, Equation 12, the liquid core does in fact contain the same order of magnitude of liquid as required by the simulation.

It is more revealing to look at the shape of the curves. In the simulation, the liquid accumulation begins to fall rapidly around 4 ms. However, all the models show the intact core length staying high, and only dropping off at a later time. Unlike the injected droplet diameter models based on instantaneous formation of droplets, the combustion models based on a large liquid core do not match the experimental data, even with scaling.

Figure 22 shows the results of the application of the same intact core formulas (Equations 8, 10, and 12) for a 155-mm firing (5-liter charge - see Figure 10). The difference in shape is even more dramatic. Also, totally different scaling factors than those used in the 30-mm simulation were required to match roughly the magnitude of the liquid accumulation. Thus, an assumption that most of the liquid accumulation is in the intact liquid core does not match the experimental data, using any of these three formulas. These formulas are based on questionable assumptions (Chatwani and Bracco 1985), and experimental studies of the intact cores of jets have only been performed at low pressures. Thus, the above study does not eliminate the possibility that there is a substantial amount of liquid in the intact core of the jet. However, at present, we are not able to model this phenomena and it is not included in our simulations.

There remains the question of why the injected droplet diameter formula in Equation 3 is applicable, with scaling, to the gun case. The droplet diameter formulas in Equations 1–3 are for droplets initially stripped off the surface of the jet and predict very small droplets. In our application we have biased the droplet diameter by ignoring the intact jet core. In addition, the sheet thickness is larger than that considered in the experiments, the gas is more dense, and the jet is axially confined. Yet, apparently, the functional relationship between dominant parameters determining injected droplet diameter in Equation 3 is approximately descriptive of the VIC cases. The fact that the 30-mm, 105-mm, and 155-mm cases are related in design and have similar injection velocity histories together with the strong dependence of droplet diameter in Equation 3 on injection velocity may explain the similarity in injected droplet diameter profiles.

9. SENSITIVE TIME LAG MODEL

The current droplet model is not completely satisfactory, since the theoretical correlation must be scaled to obtain good agreement with the experimental data. An alternate approach is developed, based on a simpler combustion model.

Liquid propellant rockets have similarities to liquid propellant guns. Crocco has developed a time lag model for combustion in a rocket (Crocco 1965; Harrje 1972). As discussed above, there are many phenomena occurring in the injection and combustion process. In Crocco's theory, all of these phenomena are lumped into a single time lag. That is, the liquid propellant is assumed to be injected and, after some specific time lag, τ, to instantaneously release all of its energy and form final products.

The simplest implementation is to assume that the time lag, τ, is a constant. In this case the governing equation is

$$m_r(t + \tau) = m_j(t), \tag{13}$$

where m_j is the injection rate (g/s) and m_r is the rate at which the propellant turns to gas and releases its energy (g/s). This is a simple extension of the instantaneous combustion model. Instead of releasing all of its energy upon injection, the liquid propellant releases all of its energy a specific time after injection.

Most lumped parameter codes with a delayed energy release keep track of the amount of propellant. That is, at the end of a time step, the injection rate is multiplied by the time step size to get the number of grams injected over the time step. Some number of time steps later, this energy is released. This discretization is not used in the present implementation. Instead, the value of the injection rate itself is stored. The energy release rate at any given time, t, is found by interpolating the injection rate vector to find the injection rate at the time, $t-\tau$.

A slightly more complex energy release model is obtained by assuming that the time lag, τ, varies with time according to some known relation. Crocco derived a governing equation

$$m_r(t + \tau)\,[1 + \partial\tau/\partial t] = m_j(t). \qquad (14)$$

The derivative of the time lag is evaluated at the time t. If the time lag is constant, this reduces to Equation 13. If the time lag is increasing, the energy release is spread out over a larger time interval than the injection, i.e., the energy release rate is smaller than the injection rate. If the time lag is decreasing, the energy release occurs over a smaller time period than the injection process, and the energy release rate is larger than the injection rate. The derivative of the time lag is found numerically.

In its final form, the time lag is assumed to be sensitive to the conditions in the chamber. That is, the time lag depends on the environment of the injected liquid between the time of injection and the time of energy release. Crocco assumed that the time lag is sensitive only to the chamber pressure. All other phenomena that affect the jet breakup and combustion are implicitly assumed to correlate with chamber pressure. Suppose that some liquid is injected at time t_1. The liquid will release its energy at a time t_2, where the integral of the pressure from t_1 to t_2 equals a specified delay constant. As the pressure increases, the time lag becomes smaller, which is qualitatively correct. Crocco also allowed the pressure to have an exponent n, which, for lack of information, is here simply set equal to one.

In liquid rockets under normal operating conditions, the chamber pressure is constant. Crocco developed the sensitive time lag theory to study the onset of instability, where chamber pressure variations are small. In a gun, the ballistic process is highly transient and changes in pressure over the ballistic cycle are large. Nevertheless, the sensitive time lag theory was integrated into the liquid gun code.

A value for the delay constant is input (units of MPa-ms). At any time t_1, the value of the injection rate is stored. A value pt_1 tracking the liquid exposure to chamber conditions is set equal to zero. At the end of each subsequent time step, the average pressure times the time increment is added to pt_1. When pt_1 becomes greater than the delay constant, the time lag $\tau(t_1)$ is found by interpolation. So the time lag value at time t_1 is not usually known until many time steps later.

Now suppose that the integration has reached a later time step t_n. The earlier time t_e is required such that $t_e + \tau(t_e) = t_n$. In general, t_e will be between two previous integration times, t_i and t_{i+1}, i.e., $t_i + \tau(t_i)$ will be less than t_n, and $t_{i+1} + \tau(t_{i+1})$ will be greater than t_n. The time, t_e, and the corresponding injection rate, $m_j(t_e)$, are found by interpolation. The derivative of the time delay is approximated by $[\tau(t_{i+1})-\tau(t_i)]/(t_{i+1}-t_i)$. Equation 14 is then used to calculate the energy release rate.

One additional complication is that the value, $\tau(t_{i+1})$, may not yet be known. In this case, $\tau(t_{i+1})$ is approximated by extrapolation of the computed time lags. Error due to this extrapolation is minor.

10. RESULTS - TIME LAG MODEL

As before, the model is first applied to the 30-mm case. A value of 30 MPa-ms for the delay constant gives the best results (Figure 23, dashed line). The sensitive time lag simulation is very similar to the simulation using the droplet combustion model (dotted line). The interior ballistics model is applied to the other three gun cases, using 30 MPa-ms for the delay constant. The overall agreement between simulated and experimental pressure versus time profiles is equivalent to that obtained using the droplet combustion model (Figures 24–26). The agreement in muzzle velocity is also good (Table 5). The largest disagreement in the maximum chamber pressures is about 4% (30-mm case).

Table 5. Muzzle Velocities Using the Sensitive Time Lag Model

Gun	Charge, l	Muzzle Velocity, Exp (m/s)	Muzzle Velocity, Model (m/s)	Percent difference
30-mm	.23	776	764	-1.5
105-mm	2.0	666	655	-1.7
155-mm	2.2	393	399	1.5
155-mm	5.2	586	592	1.0

The results are very good considering the simplicity of the model, i.e., droplet size and propellant combustion rates no longer enter into the combustion model. The results are similar for the other seven cases discussed above (not shown).

The agreement between the predicted pressure profiles from the injection model and the sensitive time lag model is very good. This is partly due to the nature of the gun configurations. The droplet size in the droplet injection model primarily depends on the velocity of the injected liquid. This velocity in turn depends on the pressure difference between the reservoir and the combustion chamber. The reservoir pressure will always be close to the chamber pressure times the hydraulic difference. So indirectly, the droplet size is most sensitive to the chamber pressure, which is also the parameter that affects the sensitive time lag model.

11. SUMMARY

A new droplet model has been introduced into the regenerative liquid propellant gun code. Unlike the previous droplet profile model, there is a single adjustable parameter. All of the Concept VIC data is represented quite well using a single value of the adjustable parameter, which was fixed in the simulation of the 30-mm test data.

Models of an intact jet core have also been studied. These models do not appear to be applicable to the gun cases considered. In general, the models predict much less accumulation, with accumulation occurring later in the ballistic cycle, than the experimental data.

An even simpler combustion model is introduced, in which the energy in the propellant is released after the cumulative pressure times time reaches a predetermined value. The results are remarkably similar to the new droplet model.

The processes in the combustion chamber are very complicated. Neither of the above models embodies the details of the injection, breakup, and combustion processes. However, for the Concept VIC guns studied, the simple models are surprisingly accurate. It is not apparent how well these models will extrapolate to different gun configurations and charge sizes.

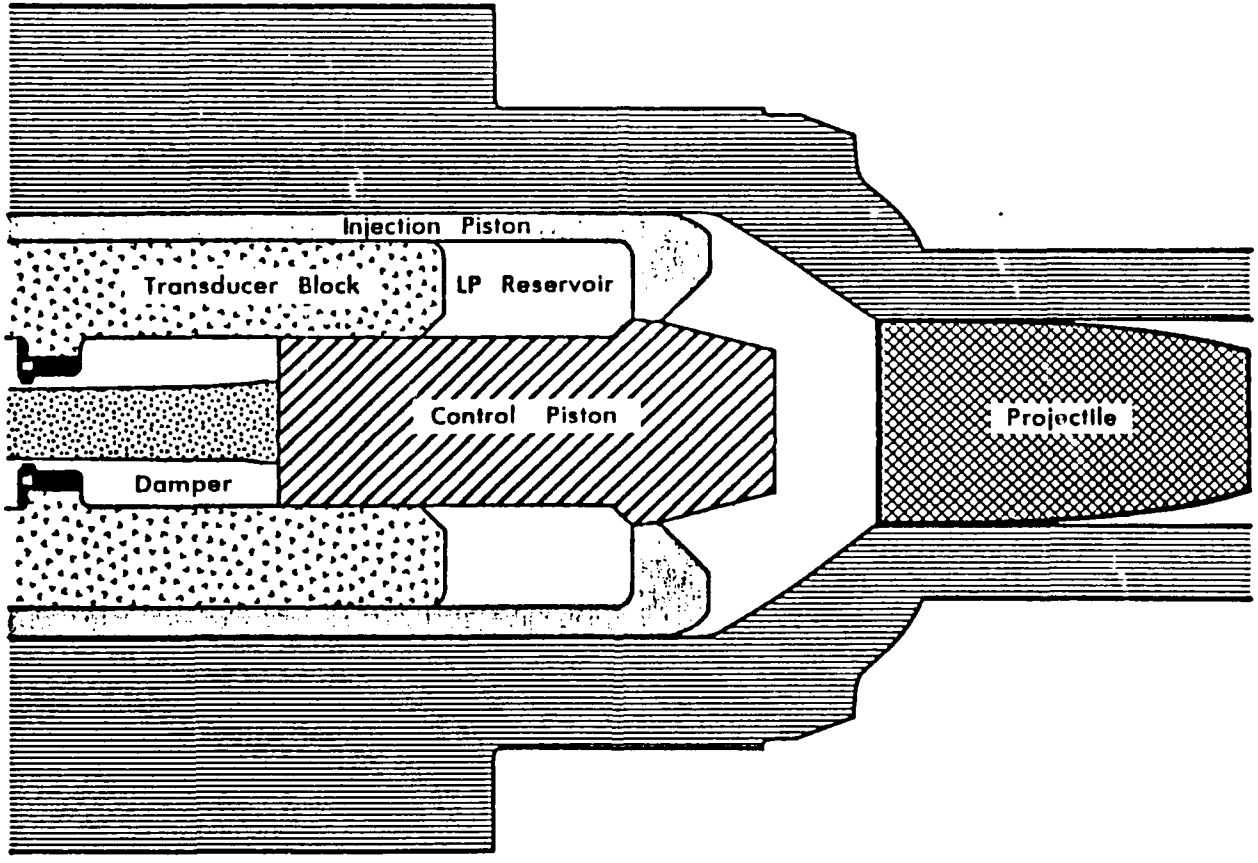

Figure 1. A Concept VIC Regenerative Liquid Propellant Gun.

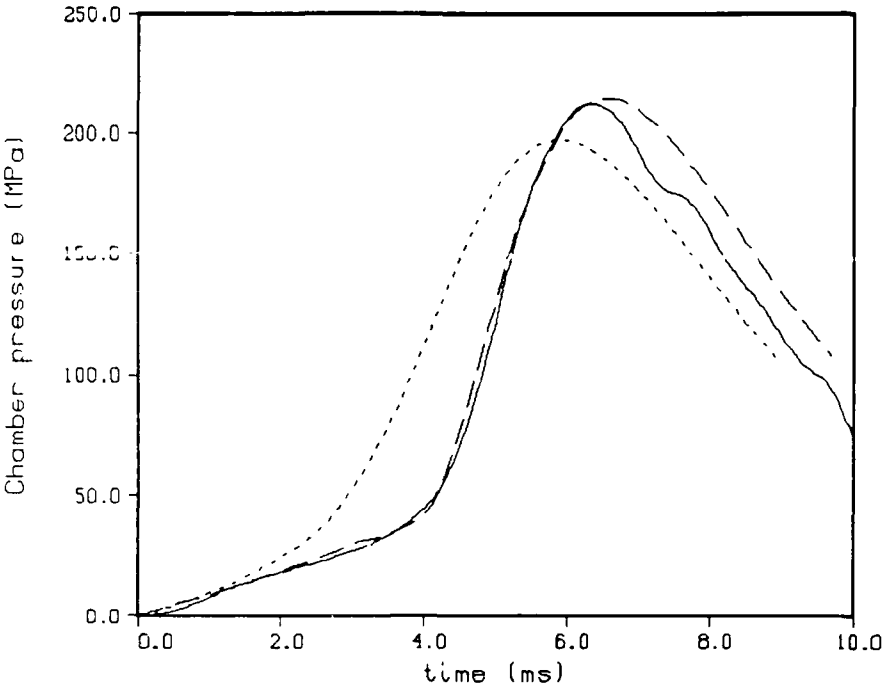

Figure 2. Combustion Chamber Pressure, 30-mm Gun, Experiment (line), Instantaneous Combustion Model (dot), 30-mm Droplet Profile (dash).

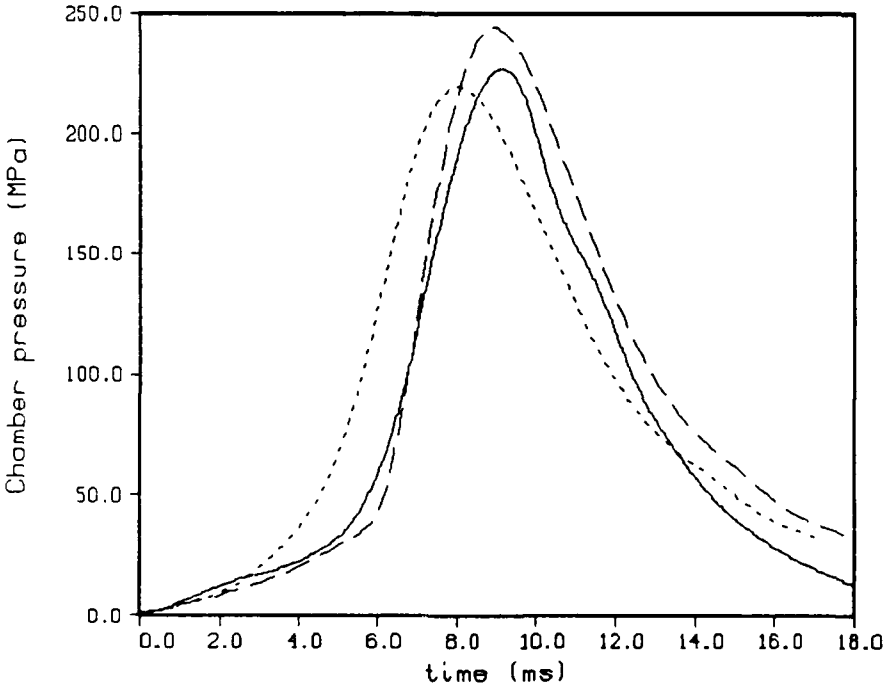

Figure 3. Combustion Chamber Pressure, 105-mm Gun, Experiment (line), Instantaneous Combustion Model (dot), 30-mm Droplet Profile (dash).

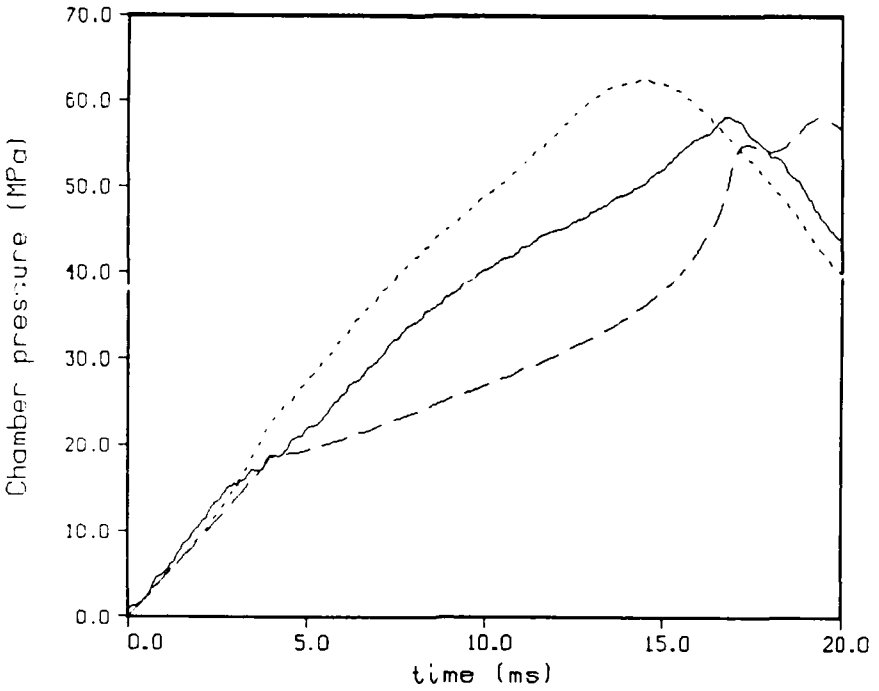

Figure 4. Combustion Chamber Pressure, 155-mm Gun - 2-Liter Charge. Experiment (line), Instantaneous Combustion Model (dot), 30-mm Droplet Profile (dash).

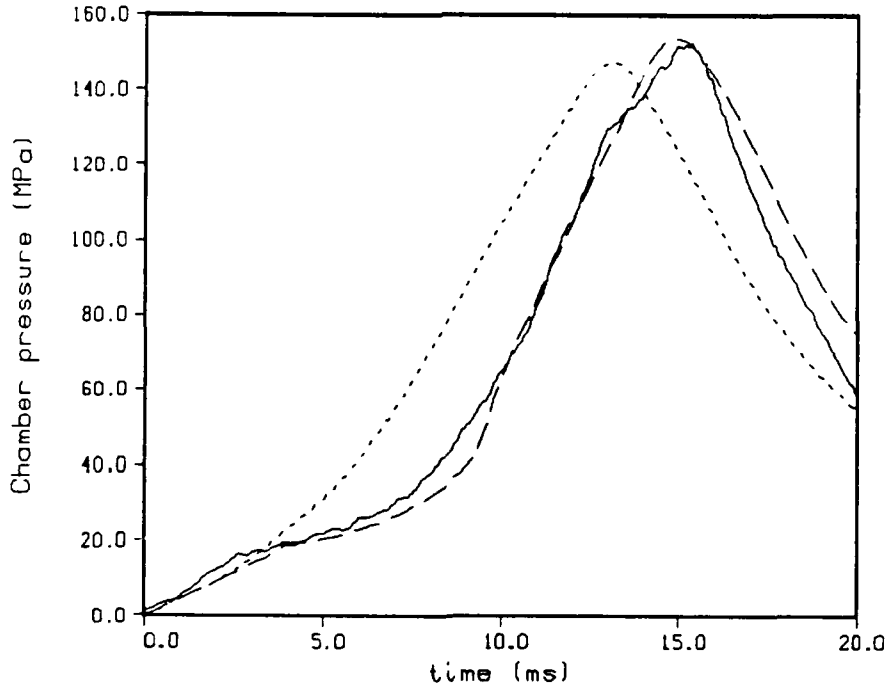

Figure 5. Combustion Chamber Pressure, 155-mm Gun - 5-Liter Charge. Experiment (line), Instantaneous Combustion Model (dot), 30-mm Droplet Profile (dash).

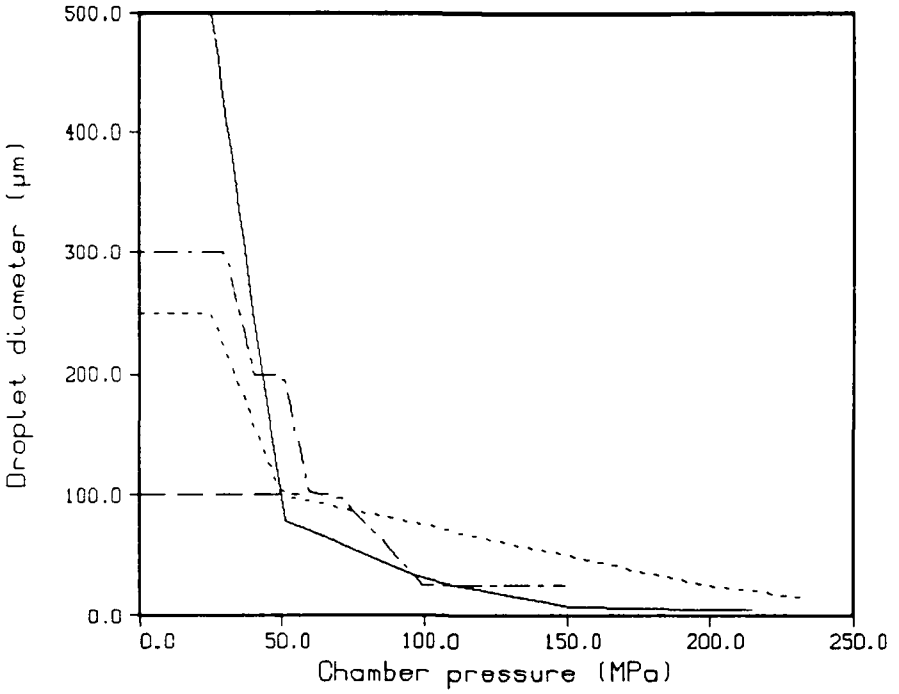

Figure 6. Empirical Droplet Diameter Profiles, 30-mm (line). 105-mm (dot). 155-mm - 2-Liter Charge (dash), 155-mm - 5-Liter Charge (dot-dash).

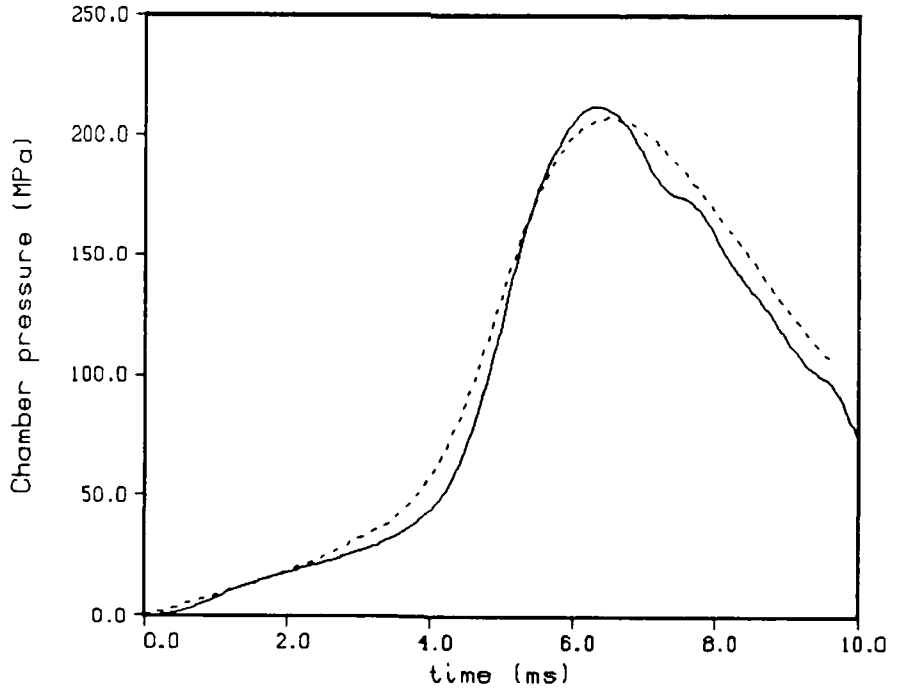

Figure 7. Combustion Chamber Pressure, 30-mm Gun. Experiment (line). Droplet Injection Model (dot).

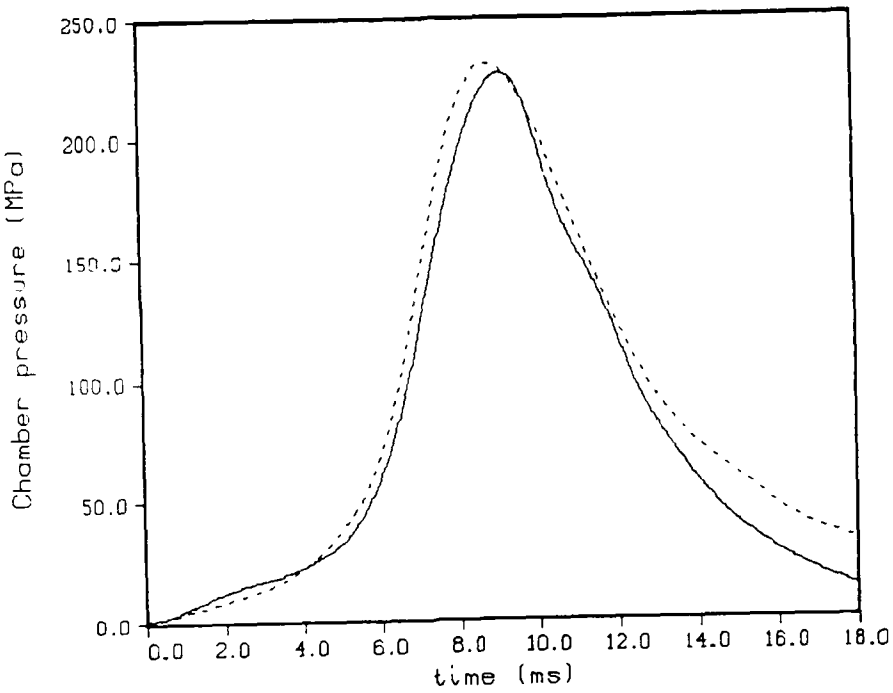

Figure 8. Combustion Chamber Pressure, 105-mm Gun. Experiment (line). Droplet Injection Model (dot).

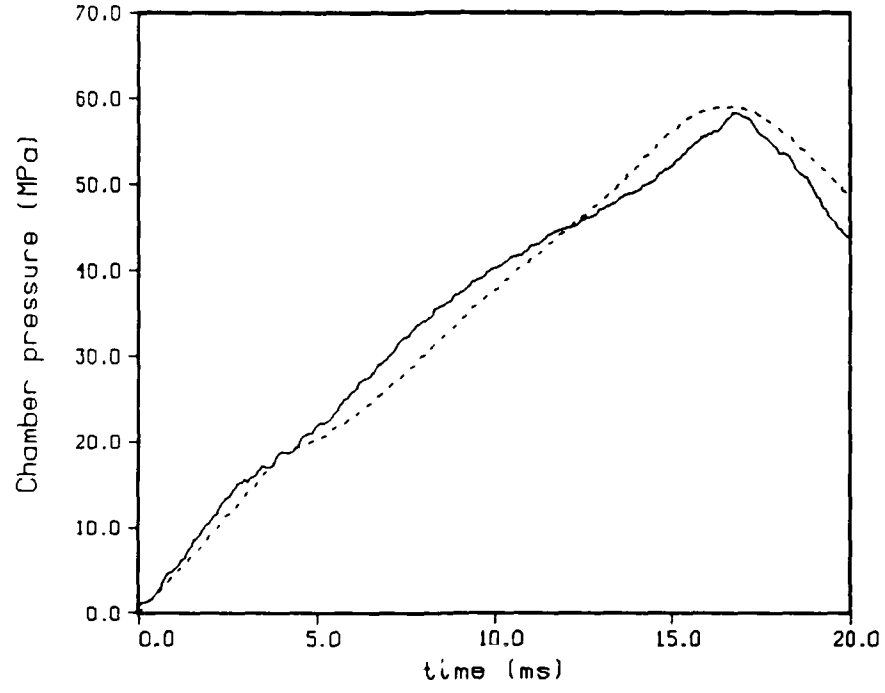

Figure 9. Combustion Chamber Pressure, 155-mm Gun - 2-Liter Charge. Experiment (line), Droplet Injection Model (dot).

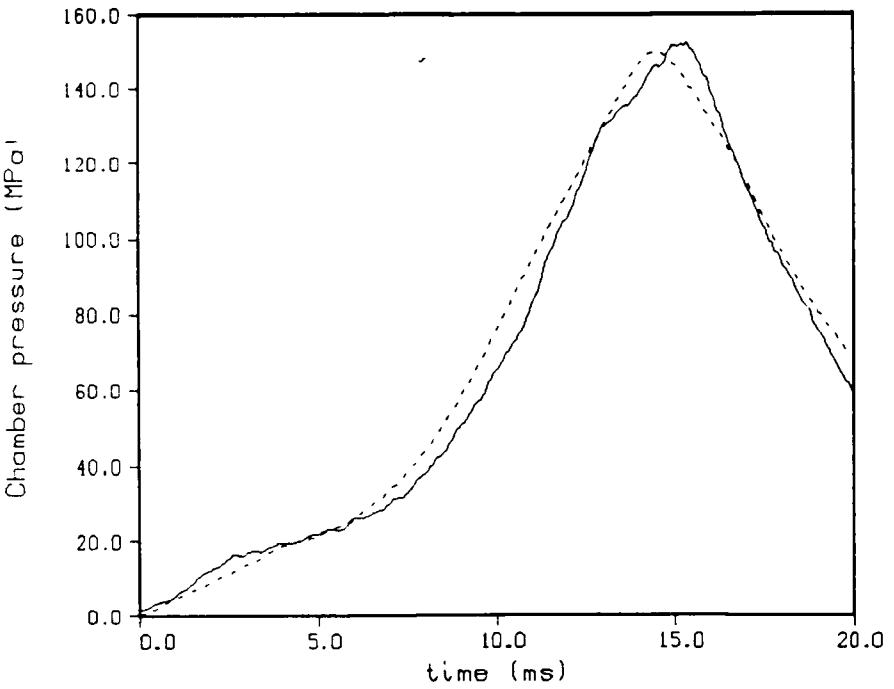

Figure 10. Combustion Chamber Pressure, 155-mm Gun - 5-Liter Charge. Experiment (line), Droplet Injection Model (dot).

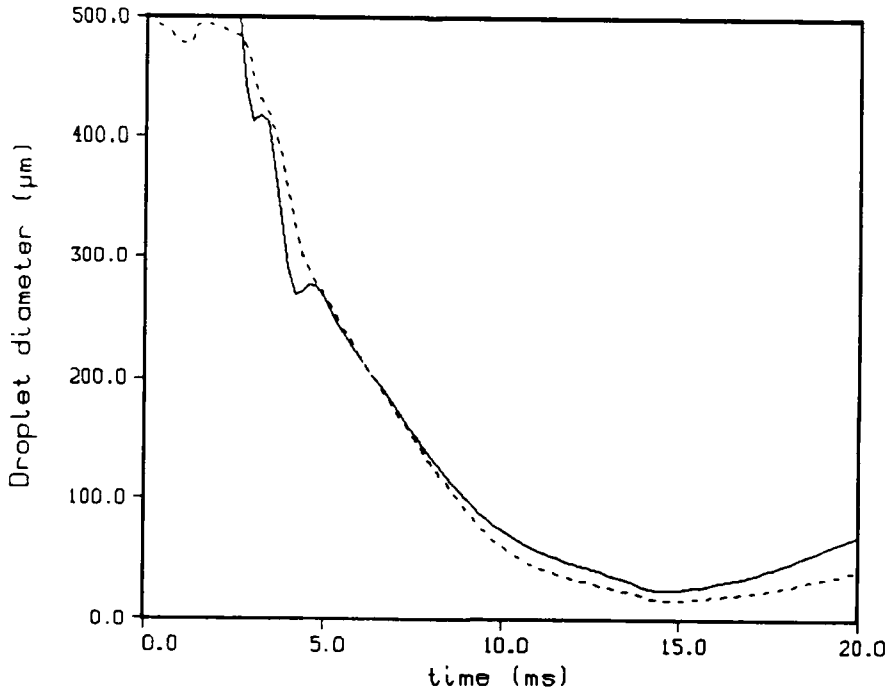

Figure 11. Droplet Injection Model, 155-mm Gun - 5-Liter Charge. Injected Droplet Diameter (line), Combustion Chamber Droplet Diameter (dot).

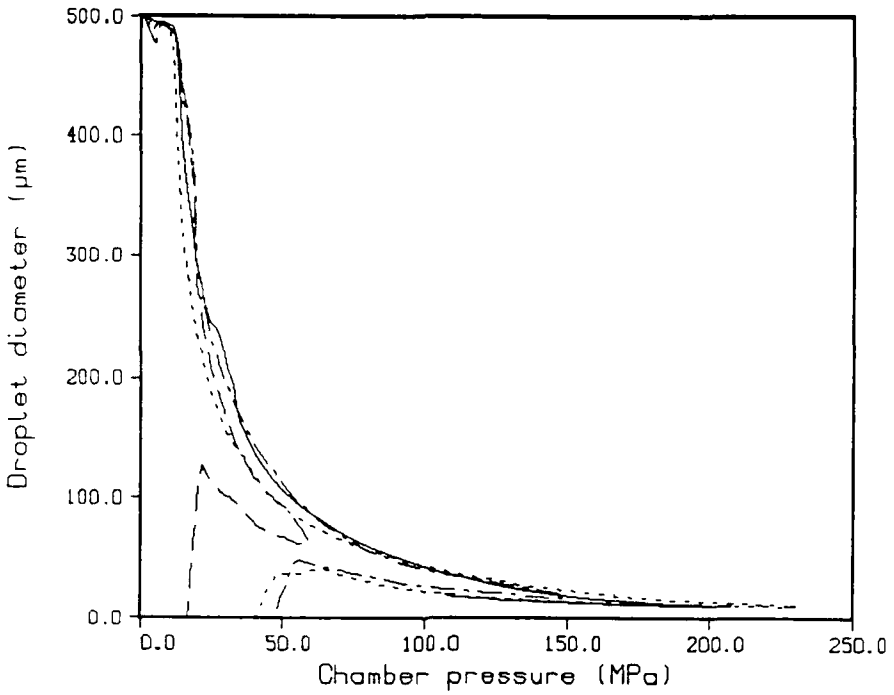

Figure 12. Droplet Injection Model, Combustion Chamber Droplet Diameter Profiles. 30-mm (line), 105-mm (dot), 155-mm - 2-Liter Charge (dash), 155-mm - 5-Liter Charge (dot-dash).

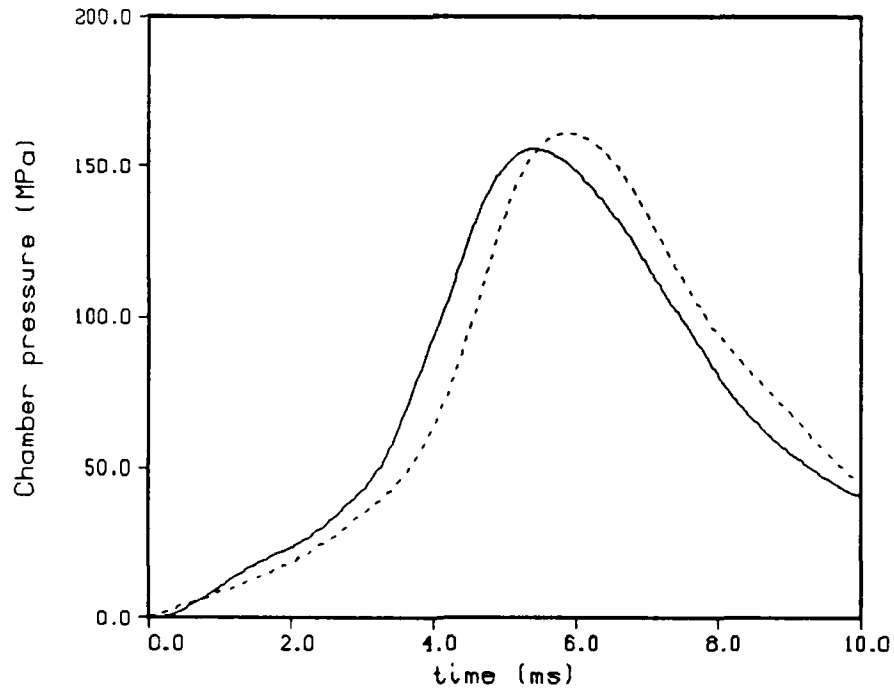

Figure 13. Combustion Chamber Pressure, 30-mm Gun - Round 15. Experiment (line), Droplet Injection Model (dot).

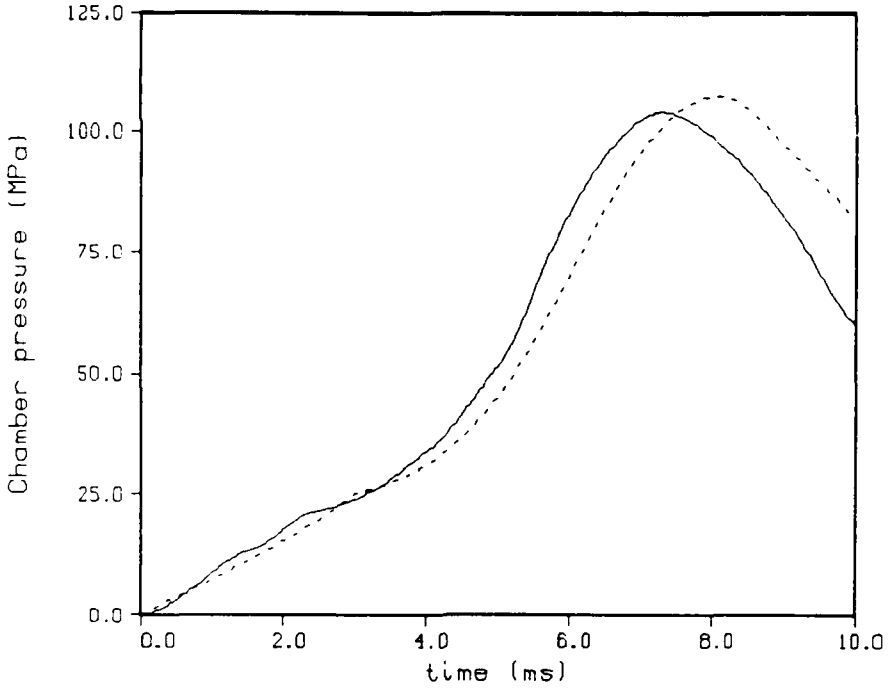

Figure 14. Combustion Chamber Pressure, 30-mm Gun - Round 22. Experiment (line), Droplet Injection Model (dot).

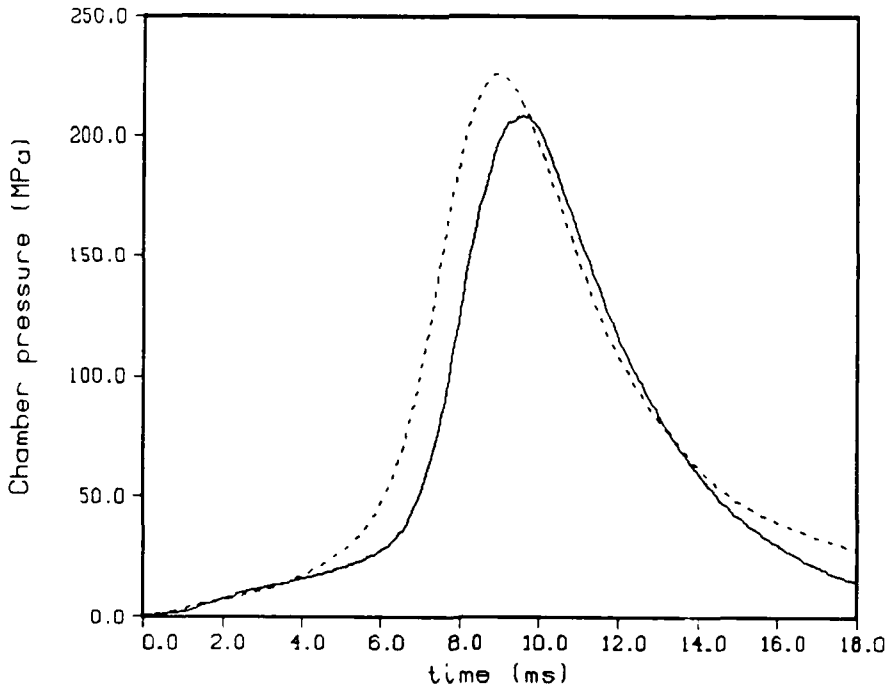

Figure 15. Combustion Chamber Pressure, 105-mm Gun - Round 15. Experiment (line), Droplet Injection Model (dot).

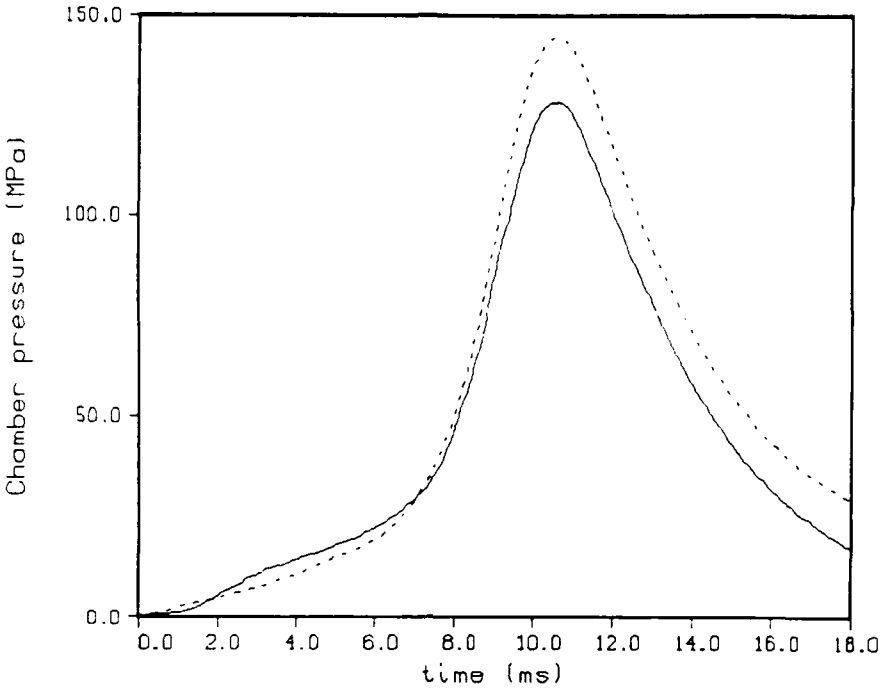

Figure 16. Combustion Chamber Pressure, 105-mm Gun - Round 7. Experiment (line), Droplet Injection Model (dot).

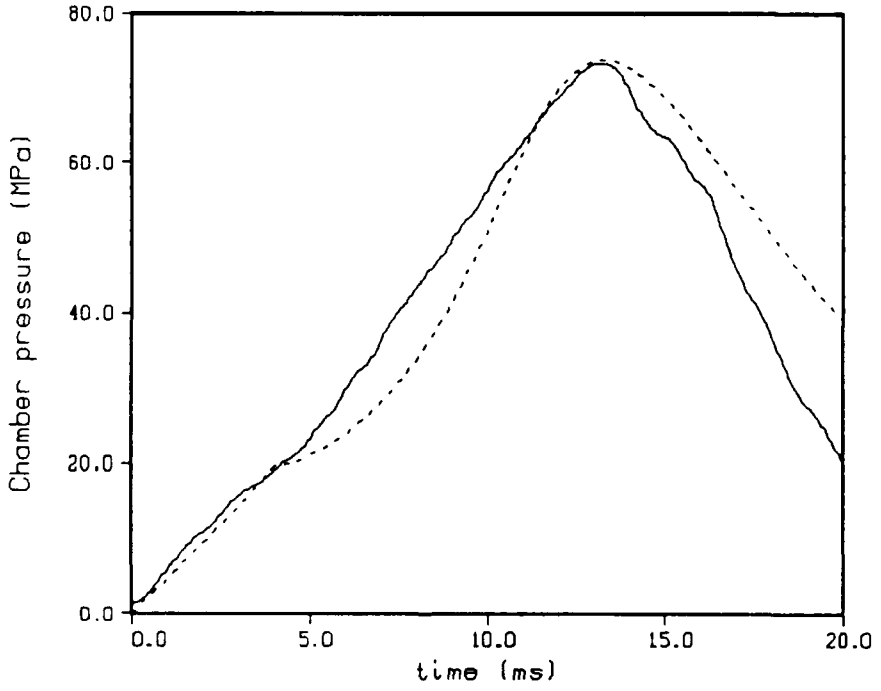

Figure 17. Combustion Chamber Pressure, 155-mm Gun - Round 17. Experiment (line), Droplet Injection Model (dot).

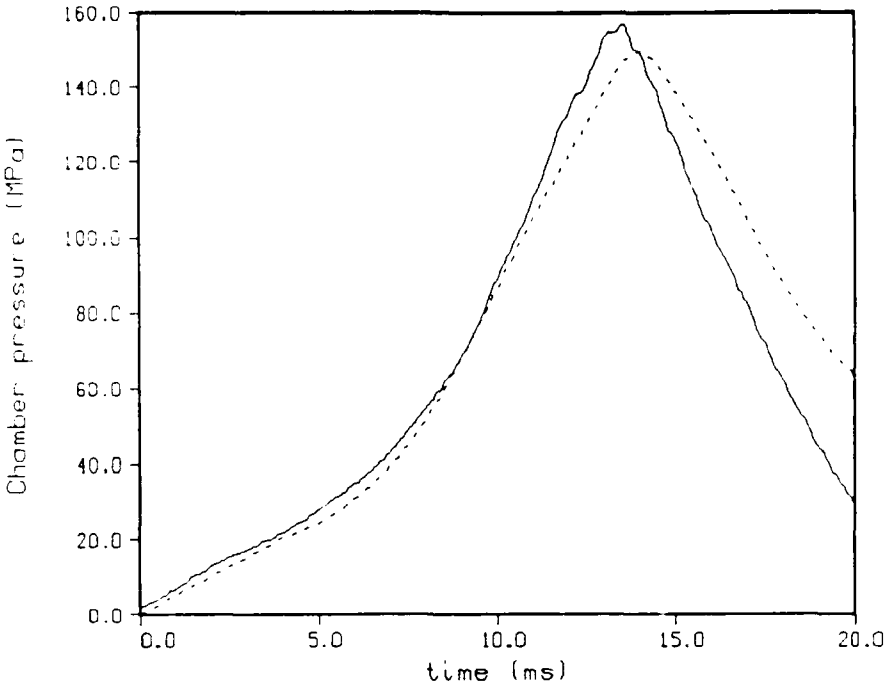

Figure 18. Combustion Chamber Pressure, 155-mm Gun - Round 58. Experiment (line), Droplet Injection Model (dot).

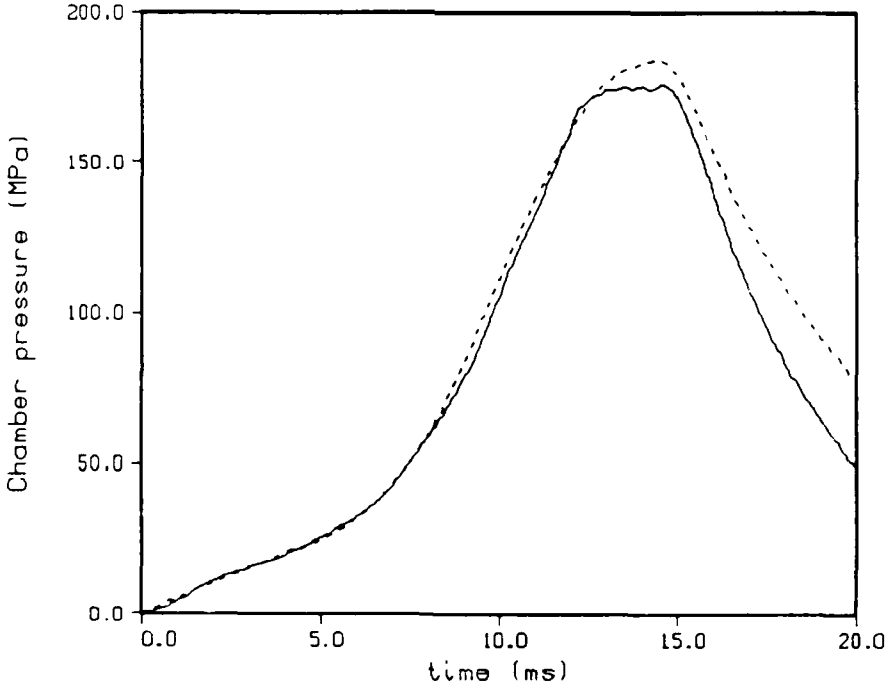

Figure 19. Combustion Chamber Pressure, 155-mm Gun - Round 65. Experiment (line), Droplet Injection Model (dot).

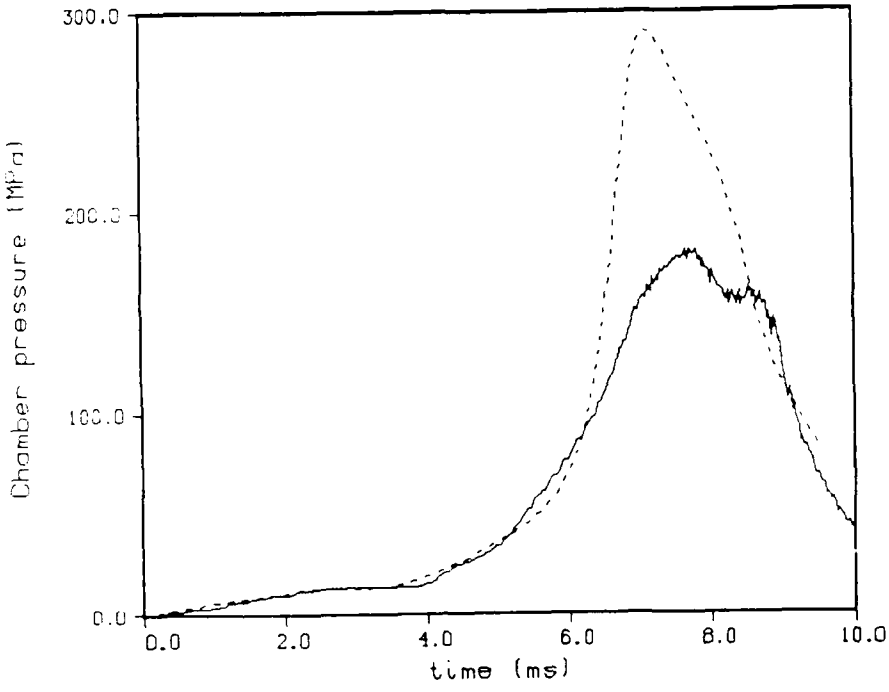

Figure 20. Combustion Chamber Pressure, 30-mm Gun - Concept VI - Round 8. Experiment (line), Droplet Injection Model (dot).

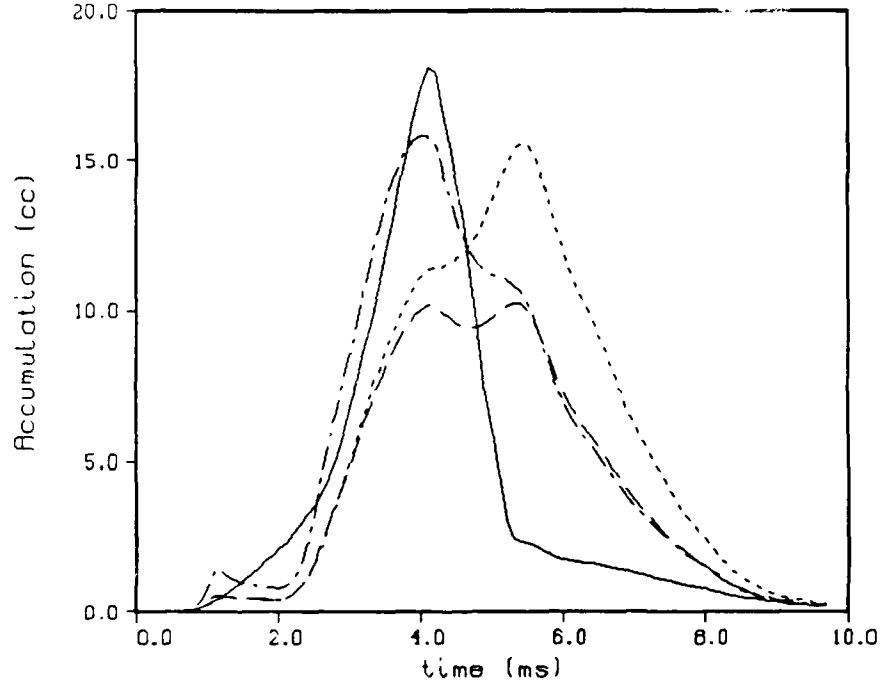

Figure 21. Liquid Accumulation, 30-mm Gun. Simulation (line), Taylor (dot), Wolfe and Andersen times 10 (dash), Mayer times 100 (dot-dash).

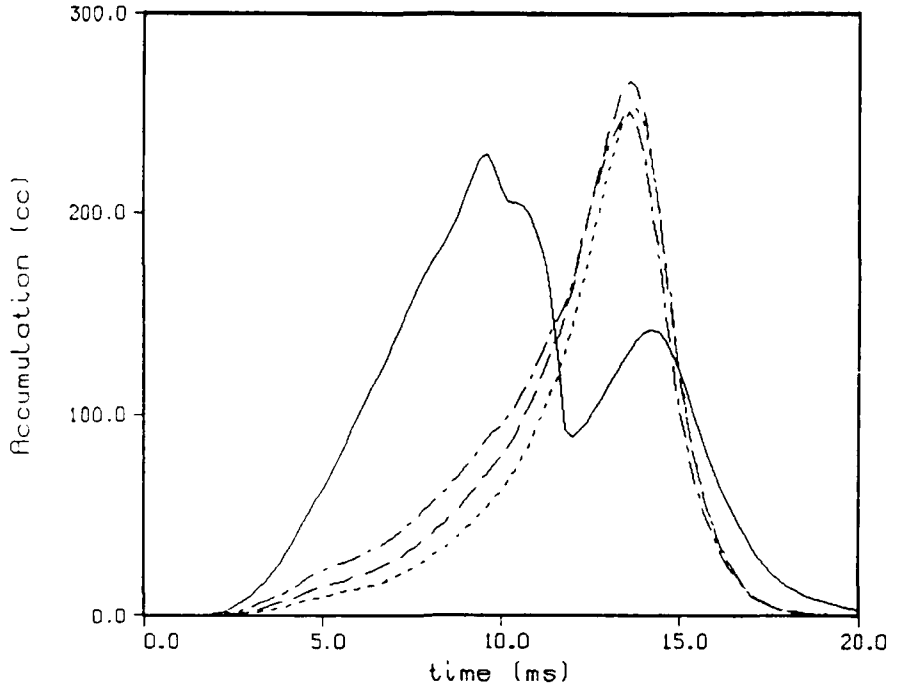

Figure 22. Liquid Accumulation, 155-mm Gun - 5 Liter Charge. Simulation (line), Taylor divided by 5 (dot), Wolfe and Andersen times 3 (dash), Mayer Times 25 (dot-dash).

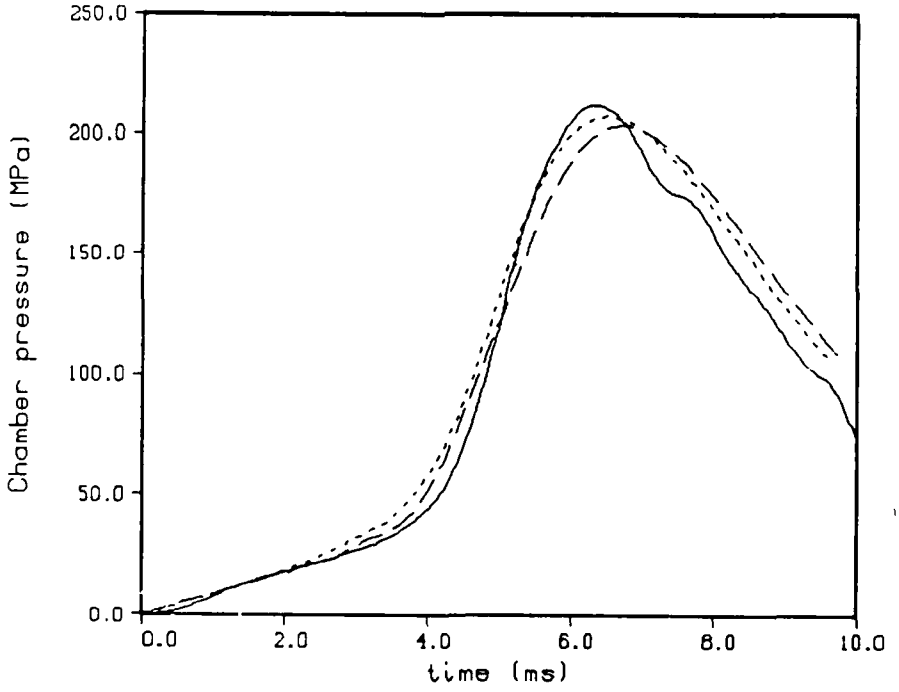

Figure 23. Combustion Chamber Pressure, 30-mm Gun. Experiment (line), Droplet Injection Model (dot), Sensitive Time Lag Model (dash).

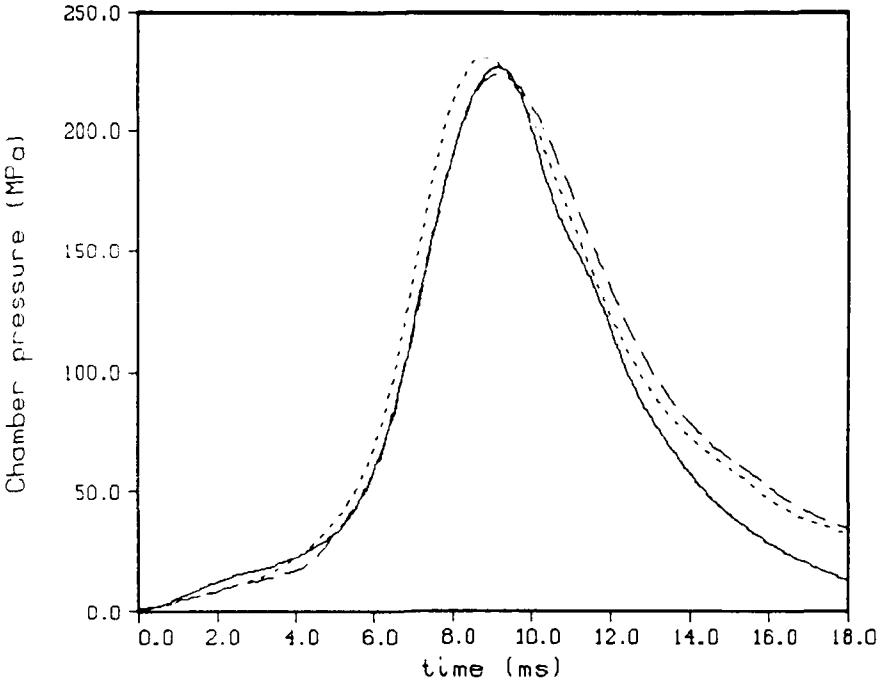

Figure 24. Combustion Chamber Pressure, 105-mm Gun. Experiment (line), Droplet Injection Model (dot), Sensitive Time Lag Model (dash).

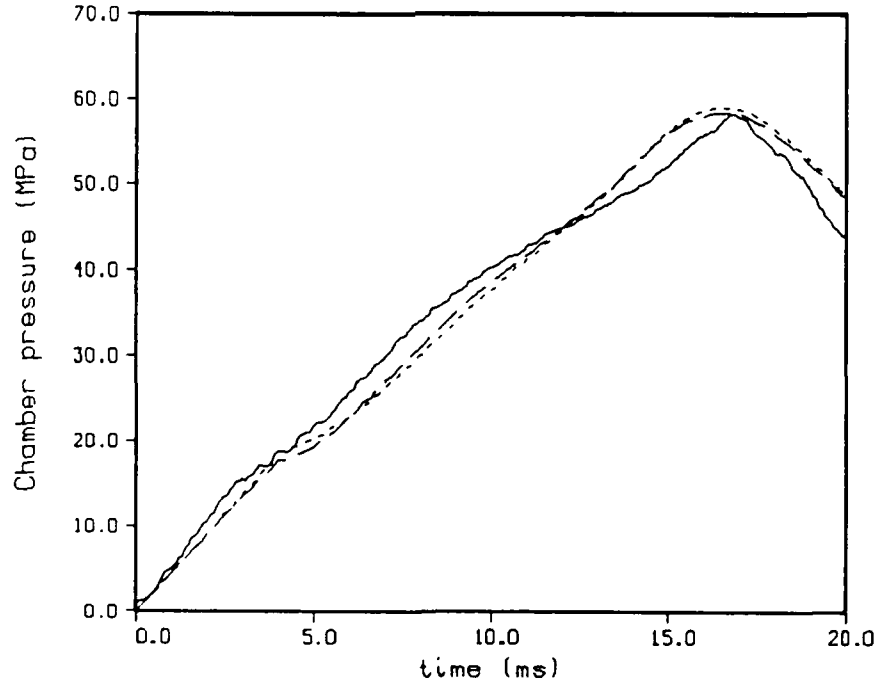

Figure 25. Combustion Chamber Pressure, 155-mm Gun - 2-Liter Charge. Experiment (line), Droplet Injection Model (dot), Sensitive Time Lag Model (dash).

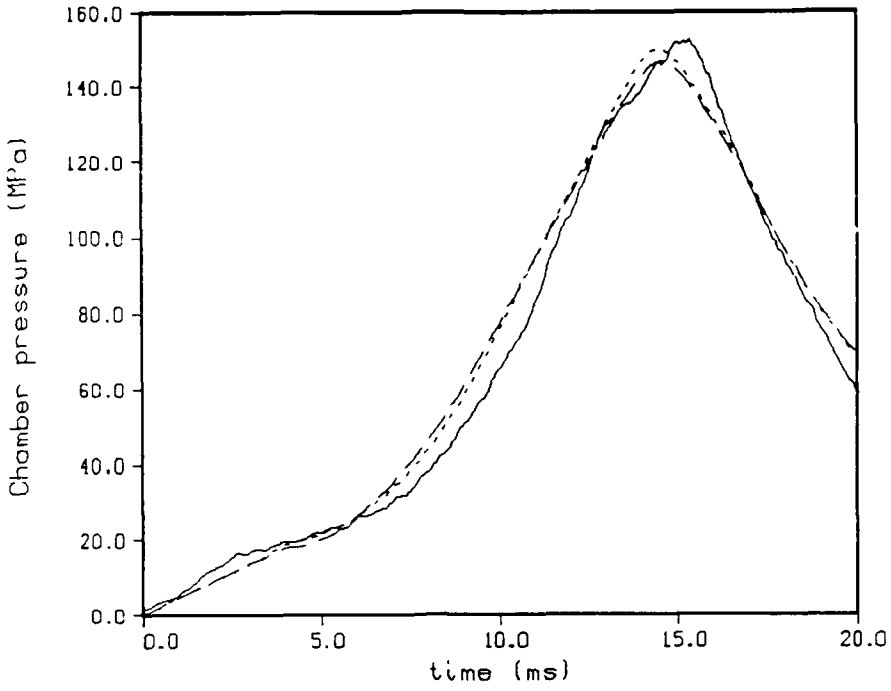

Figure 26. Combustion Chamber Pressure, 155-mm Gun - 5-Liter Charge. Experiment (line), Droplet Injection Model (dot), Sensitive Time Lag Model (dash).

INTENTIONALLY LEFT BLANK.

12. REFERENCES

Chatwani, A. U., and F. V. Bracco. "Computation of Dense Spray Jets." 3rd International Conference on Liquid Atomization and Spray Systems, Imperial College, London, July 1985.

Coffee, T. P. "A Lumped Parameter Code for Regenerative Liquid Propellant Guns." BRL-TR-2703, U.S. Army Ballistic Research Laboratory, Aberdeen Proving Ground, MD, December 1985.

Coffee, T. P. "An Updated Lumped Parameter Code for Regenerative Liquid Propellant In-Line Guns." BRL-TR-2974, U.S. Army Ballistic Research Laboratory, Aberdeen Proving Ground, MD, December 1988.

Coffee, T. P., G. P. Wren, and W. F. Morrison. "A Comparison Between Experiment and Simulation for Concept VIC Regenerative Liquid Propellant Guns. I. 30 mm." BRL-TR-3072, U.S. Army Ballistic Research Laboratory, Aberdeen Proving Ground, MD, December 1989.

Coffee, T. P., G. P. Wren, and W. F. Morrison. "A Comparison Between Experiment and Simulation for Concept VIC Regenerative Liquid Propellant Guns. II. 105 mm." BRL-TR-3093, U.S. Army Ballistic Research Laboratory, Aberdeen Proving Ground, MD, March 1990.

Crocco, L. "Theoretical Studies on Liquid-Propellant Rocket Instability." Tenth Symposium (International) on Combustion, pp. 1101-1128, The Combustion Institute, 1965.

Faeth, G. M. "Evaporation and Combustion of Sprays." Prog. Energy Combust. Sci., Vol. 9, pp. 1-76, 1983.

Harrje, D. T. "Liquid Propellant Rocket Combustion Instability." NASA SP-194, Washington, D.C., 1972.

Mayer, E. "Theory of Liquid Atomization in High Velocity Gas Streams." ARS Journal, Vol. 31, p. 1783, 1961.

McBratney, W. F. "Windowed Chamber Investigation of the Burning Rate of Liquid Monopropellant for Guns." ARBRL-MR-03018, U.S. Army Ballistic Research Laboratory, Aberdeen Proving Ground, MD, April 1980.

McBratney, W. F. "Burning Rate Data, LPG 1845." ARBRL-MR-03128, U.S. Army Ballistic Research Laboratory, Aberdeen Proving Ground, MD, August 1981.

Morrison, W. F., and T. P. Coffee. "A Modified Lagrange Pressure Gradient for the Regenerative Liquid Propellant Gun." BRL-TR-3073, U.S. Army Ballistic Research Laboratory, Aberdeen Proving Ground, MD, January 1990.

Weiss, M. A., and C. H. Worsham. "Atomization in High Velocity Airstreams." ARS Journal Vol. 29, p. 252, 1959.

Wolfe, H. E., and W. H. Andersen. "Kinetics, Mechanism, and Resultant Droplet Sizes of the Aerodynamic Breakup of Liquid Drops." Aerojet Report No. 0395-04(18)SP, April 1964.

Wren, G. P., T. P. Coffee, and W. F. Morrison. "A Comparison Between Experiment and Simulation for Concept VIC Regenerative Liquid Propellant Guns. III. 155 mm." BRL-TR-3151, U.S. Army Ballistic Research Laboratory, Aberdeen Proving Ground, MD, September 1990.

INTENTIONALLY LEFT BLANK.

GLOSSARY

A_v	vent area of the injector, cm^2.
d_3	mean diameter of droplets in the chamber, cm.
d_4	mean diameter of droplets in the tube, cm.
d_j	mean diameter of the drops injected into the chamber, cm.
d_{j4}	mean diameter of the drops injected into the gun tube, cm.
D	diameter of a circular or annular injector, cm.
D_h	hydraulic diameter of an annular injector, cm.
m_{13}	the rate of mass injection from the reservoir, g/s.
m_{34}	the rate of mass injection into the gun tube, g/s.
m_3	the rate of combustion of the liquid in the chamber, g/s.
m_4	the rate of combustion of the liquid in the tube, g/s.
M_3	the total mass in the chamber, g.
M_{L3}	the mass of all the liquid in the chamber, g.
m_j	injection rate for a generic injector, g/s.
m_r	energy release rate for a propellant, g/s.
S_3	surface area of the drops in the chamber, cm^2.
S_4	surface area of the drops in the tube, cm^2.
t_b	breakup time of a jet, s.
V	relative velocity between gas and liquid, cm/s.
x_b	breakup length of a jet, cm.
μ_L	liquid dynamic viscosity, poise = g/cm-s.
μ_G	gas dynamic viscosity, poise = g/cm-s.
ρ_L	liquid density, g/cm^3.

ρ_{L3} density of the liquid in the chamber, g/cm^3.

ρ_{L4} average density of the liquid in the gun tube, g/cm^3.

ρ_G gas density, g/cm^3.

ρ_{GO} gas density at atmospheric pressure and room temperature, g/cm^3.

σ_L surface tension of the liquid, dynes/cm = g/s^2.

τ time delay between injection and energy release, s.

INTENTIONALLY LEFT BLANK.

No of Copies	Organization
2	Administrator Defense Technical Info Center ATTN: DTIC-DDA Cameron Station Alexandria, VA 22304-6145
1	HQDA (SARD-TR) WASH DC 20310-0001
1	Commander U.S. Army Materiel Command ATTN: AMCDRA-ST 5001 Eisenhower Avenue Alexandria, VA 22333-0001
1	Commander U.S. Army Laboratory Command ATTN: AMSLC-DL 2800 Powder Mill Road Adelphi, MD 20783-1145
2	Commander U.S. Army Armament Research, Development, and Engineering Center ATTN: SMCAR-IMI-I Picatinny Arsenal, NJ 07806-5000
2	Commander U.S. Army Armament Research, Development, and Engineering Center ATTN: SMCAR-TDC Picatinny Arsenal, NJ 07806-5000
1	Director Benet Weapons Laboratory U.S. Army Armament Research, Development, and Engineering Center ATTN: SMCAR-CCB-TL Watervliet, NY 12189-4050
1	Commander U.S. Army Armament, Munitions and Chemical Command ATTN: SMCAR-ESP-L Rock Island, IL 61299-5000
1	Director U.S. Army Aviation Research and Technology Activity ATTN: SAVRT-R (Library) M/S 219-3 Ames Research Center Moffett Field, CA 94035-1000

No of Copies	Organization
1	Commander U.S. Army Missile Command ATTN: AMSMI-RD-CS-R (DOC) Redstone Arsenal, AL 35898-5010
1	Commander U.S. Army Tank-Automotive Command ATTN: ASQNC-TAC-DIT (Technical Information Center) Warren, MI 48397-5000
1	Director U.S. Army TRADOC Analysis Command ATTN: ATRC-WSR White Sands Missile Range, NM 88002-5502
(Class. only)1	Commandant U.S. Army Infantry School ATTN: ATSH-CD (Security Mgr.) Fort Benning, GA 31905-5660
(Unclass. only)1	Commandant U.S. Army Infantry School ATTN: ATSH-CD-CSO-OR Fort Benning, GA 31905-5660
1	Air Force Armament Laboratory ATTN: AFATL/DLODL Eglin AFB, FL 32542-5000
	Aberdeen Proving Ground
2	Dir, USAMSAA ATTN: AMXSY-D AMXSY-MP, H. Cohen
1	Cdr, USATECOM ATTN: AMSTE-TD
3	Cdr, CRDEC, AMCCOM ATTN: SMCCR-RSP-A SMCCR-MU SMCCR-MSI
1	Dir, VLAMO ATTN: AMSLC-VL-D
10	Dir, BRL ATTN: SLCBR-DD-T

No. of
Copies Organization

10 Commander
US Army, ARDEC
ATTN: SMCAR-AEE-BR
B. Brodman
W. Seals
A. Beardell
SMCAR-AEE-B, D. Downs
SMCAR-AEE
A. Bracuti
D. Chieu
J. Salo
SMCAR-FSS-D, L. Frauen
SMCAR-FSA-S, H. Liberman
Picatinny Arsenal, NJ 07806-5000

3 Commander
US Army, ARDEC
ATTN: SMCAR-FSS-DA, Bldg 94
J. Feneck
R. Kopmann
J. Irizarry
Picatinny Arsenal, NJ 07806-5000

1 Commander
US Army Belvoir R&D Center
ATTN: STRBE-WC
Tech Library (Vault) B-315
Fort Belvoir, VA 22060-5606

1 Commander
US Army Research Office
ATTN: Tech Library
P.O. Box 12211
Research Triangle Park, NC 27709-2211

1 Commander
US Army, ARDEC
ATTN: SMCAR-CCS-C, T. Hung
Picatinny Arsenal, NJ 07806-5000

2 Commandant
US Army Field Artillery School
ATTN: ATSF-CMW
ATSF-TSM-CN, J. Spicer
Ft. Sill, OK 73503

No. of
Copies Organization

1 Commandant
US Army Armor Center
ATTN: ATSB-CD-MLD
Ft. Knox, KY 40121

1 Commander
Naval Surface Warfare Center
ATTN: Code G31, D.A. Wilson
Dahlgren, VA 22448-5000

1 Commander
Naval Surface Warfare Center
ATTN: Code G33, J. East
Dahlgren, VA 22448-5000

2 Commander
Naval Surface Warfare Center
ATTN: O. Dengel
K. Thorsted
Silver Spring, MD 20902-5000

1 Commander
Naval Weapons Center
China Lake, CA 93555-6001

1 Superintendent
Naval Postgraduate School
Dept of Mechanical Engr
ATTN: Code 1424, Library
Monterey, CA 93943

1 OSD/SIDO/IST
ATTN: Dr. Len Caveny
Pentagon
Washington, DC 20301-7100

1 Commandant
USAFAS
ATTN: ATSF-TSM-CN
Fort Sill, OK 73503-5600

1 Director
Jet Propulsion Lab
ATTN: Tech Library
4800 Oak Grove Drive
Pasadena, CA 91109

No. of
Copies Organization

1 Director
National Aeronautics and Space Administration
Manned Spacecraft Center
Houston, TX 77058

2 Director
National Aeronautics and Space Administration
ATTN: MS-603, Tech Library
MS-86, Dr. Povinelli
21000 Brookpark Road
Lewis Research Center
Cleveland, OH 44135

1 Director
Applied Physics Laboratory
The Johns Hopkins University
Johns Hopkins Road
Laurel, MD 20707

1 Sandia National Laboratory
Division 8152
ATTN: Dr. Ray Rychnovsky
P.O. Box 969
Livermore, CA 94551-0969

1 Sandia National Laboratory
Division 8244
ATTN: Dr. Stuart Griffiths
P.O. Box 969
Livermore, CA 94551-0969

2 Princeton Combustion Research Laboratories, Inc.
ATTN: N.A. Messina
M. Summerfield
4275 US Highway One North
Monmouth Junction, NJ 08852

1 School of Engineering and Computer Science
California State University, Sacramento
ATTN: Dr. Frederick Reardon
6000 J Street
Sacramento, CA 95819-2694

No. of
Copies Organization

1 University of Colorado at Boulder
Department of Mechanical Engineering
Engineering Center ME 1-13
ATTN: Dr. John Daily
Campus Box 427
Boulder, CO 80309-0427

1 U. of Illinois at Chicago
ATTN: Professor Sohail Murad
Dept of Chemical Engr
Box 4348
Chicago, IL 60680

1 U. of MD at College Park
ATTN: Professor Franz Kasler
Dept of Chemistry
College Park, MD 20742

1 U. of Michigan
ATTN: Professor Gerard M. Faeth
Dept of Aerospace Engr
Ann Arbor, MI 48109-3796

1 U. of Missouri at Columbia
ATTN: Professor F.K. Ross
Research Reactor
Columbia, MO 65211

1 U. of Missouri at Kansas City
Dept of Physics
ATTN: Professor R.D. Murphy
1110 East 48th Street
Kansas City, MO 64110-2499

1 Pennsylvania State University
Dept of Mechanical Engr
ATTN: Professor K. Kuo
University Park, PA 16802

1 University of Arkansas
Dept of Chemical Engr
ATTN: J. Havens
227 Engineering Bldg
Fayetteville, AR 72701

No. of
Copies Organization

3 University of Delaware
Dept of Chemistry
ATTN: Mr. James Cronin
Professor Thomas Brill
Newark, DE 19711

1 U. of Texas at Austin
Bureau of Engineering Research
ATTN: BRC EME136, Room 1.100
H. Fair
10 00 Burnet Road
Austin, TX 78758

1 Calspan Corporation
ATTN: Tech Library
P.O. Box 400
Buffalo, NY 14225

7 General Electric Ord Sys Div
ATTN: J. Mandzy, OP43-220
R.E. Mayer
W. Pasko
R. Pate
I. Magoon
Lou Ann Walter
J. McCaleb
100 Plastics Avenue
Pittsfield, MA 01201-3698

1 IITRI
ATTN: Library
10 W. 35th St.
Chicago, IL 60616

1 Paul Gough Associates, Inc.
ATTN: Dr. Paul Gough
1048 South Street
Portsmouth, NH 03801-5423

1 Science Applications Int'l Corporation
ATTN: Norman Banks
4900 Waters Edge Drive
Suite 255
Raleigh, NC 27606

1 Sundstrand Aviation Operations
ATTN: Mr. Owen Briles
P.O. Box 7202
Rockford, IL 61125

No. of
Copies Organization

1 Veritay Technology, Inc.
ATTN: E.B. Fisher
4845 Millersport Highway
P.O. Box 305
East Amherst, NY 14051-0305

1 Conway Enterprises
ATTN: Prof. Alistair Macpherson
499 Pine Top Trail
Bethlehem, PA 18017-1828

No. of Copies	Organization
1	GS2 Division Building R31 RARDE ATTN: Dr. Clive Woodley Ft. Halstead Sevenoaks, Kent TN14 7BT England

INTENTIONALLY LEFT BLANK.

USER EVALUATION SHEET/CHANGE OF ADDRESS

This laboratory undertakes a continuing effort to improve the quality of the reports it publishes. Your comments/answers below will aid us in our efforts.

1. Does this report satisfy a need? (Comment on purpose, related project, or other area of interest for which the report will be used.) _____

2. How, specifically, is the report being used? (Information source, design data, procedure, source of ideas, etc.) _____

3. Has the information in this report led to any quantitative savings as far as man-hours or dollars saved, operating costs avoided, or efficiencies achieved, etc? If so, please elaborate. _____

4. General Comments. What do you think should be changed to improve future reports? (Indicate changes to organization, technical content, format, etc.) _____

BRL Report Number BRL-TR-3223 Division Symbol _____

Check here if desire to be removed from distribution list. ____

Check here for address change. ____

Current address: Organization _____
Address _____

DEPARTMENT OF THE ARMY
Director
U.S. Army Ballistic Research Laboratory
ATTN: SLCBR-DD-T
Aberdeen Proving Ground, MD 21005-5066

OFFICIAL BUSINESS

BUSINESS REPLY MAIL
FIRST CLASS PERMIT No 0001, APG, MD

Postage will be paid by addressee.

Director
U.S. Army Ballistic Research Laboratory
ATTN: SLCBR-DD-T
Aberdeen Proving Ground, MD 21005-5066

NO POSTAGE
NECESSARY
IF MAILED
IN THE
UNITED STATES